

# Chapter 2

## Fundamentals of Electrochemistry, Corrosion and Corrosion Protection

Christian D. Fernández-Solis, Ashokanand Vimalanandan,  
Abdulrahman Altin, Jesus S. Mondragón-Ochoa, Katharina Kreth,  
Patrick Keil and Andreas Erbe

**Abstract** This chapter introduces the basics of electrochemistry, with a focus on electron transfer reactions. We will show that the electrode potential formed when a metal is immersed in a solution is most of the time not an equilibrium potential, but a mixed potential in a stationary state. This mixed potential formation is the basis of corrosion of metals in aqueous solutions. Organic coatings are introduced as protecting agents, and several types of coatings are discussed: classical passive coatings, and active coatings as modern developments. Three electrochemical techniques, which are commonly used to assess the protecting properties of coatings, are shortly introduced as well: linear polarisation measurements, electrochemical impedance spectroscopy, and scanning Kelvin probe measurements.

### 2.1 Basics of Electrochemistry

Electron transfer reactions are wide-spread in nature, e.g. in the respiratory chain, they are important technologically, e.g. in electrolyzers and for metal plating, and they contribute to the degradation of materials, in corrosion processes of metals. This chapter shall serve as an introductory text into the basic concepts, with a special focus on their importance in the field of corrosion science. Electrochemistry is quite an old science, and hence a number of good textbooks are available for more detailed introductions of the fundamental concepts [1–3]. It is worth pointing out that there are practically important corrosion mechanisms which are not at all based on electrochemical reactions. Details are available in dedicated textbooks [4, 5].

---

C.D. Fernández-Solis · A. Vimalanandan · A. Altin · J.S. Mondragón-Ochoa · A. Erbe (✉)  
Max-Planck-Institut für Eisenforschung GmbH, Max-Planck-Str. 1,  
40237 Düsseldorf, Germany  
e-mail: a.erbe@mpie.de

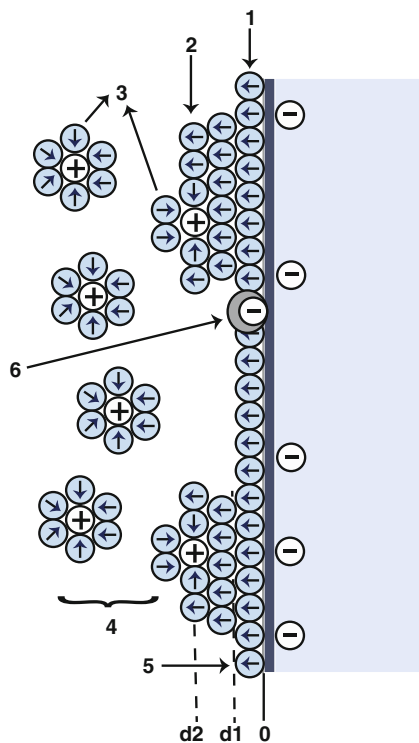
K. Kreth · P. Keil  
BASF Coatings GmbH, 48165 Münster, Germany

### 2.1.1 Electrostatic Potentials at Interfaces

Interfaces, in particular aqueous interfaces, are almost always charged, e.g. by dissociation of surface groups, or adsorption of ions from solution. On conductive substrates, the charge state of an interface may be actively controlled, as will be discussed below. Around charged interfaces, a static electric field is present, which affects the distribution of ions in solution around this interface. The rather complex multibody-interactions between solvent, mobile charges on both sides of the phase boundary, and stationary atoms leads to a complicated interfacial structure, which is schematically shown in Fig. 2.1 [6]. This interface is often referred to by the misleading term “double layer” (see also Chap. 4 by G. H. Findenegg).

Closest to the interface is a structured layer containing adsorbed molecules of the solvent and other adsorbed species. The region where the electric charges of the adsorbed ions are allocated is called inner Helmholtz layer; this region is at a distance  $d_1$  (Fig. 2.1). Solvated ions can approach the interface up to a distance  $d_2$ . The region where the electric charges of the solvated ions are located is called outer Helmholtz layer. Due to thermal motion in the system, these solvated ions are distributed in a three dimensional region ranging from the outer Helmholtz layer to the bulk. This region is often referred to as “diffuse layer”. Counter-ion distribution

**Fig. 2.1** Schematic representation of the layers at a solid/liquid interface. 1 Inner Helmholtz layer, 2 Outer Helmholtz layer, 3 Solvated ions (cations), 4 Diffuse layer, 5 Electrolyte solvent, 6 Specifically adsorbed ions. Drawing inspired by [7]



in the diffuse layer is important for some processes at a variety of interfaces (e.g., solid electrodes, biomolecules, etc.) and in technological applications as well (e.g., corrosion, paints, etc.). A simple quantitative approach to the description of the diffuse layer, balancing entropy against mean-field electrostatic attraction, is the Poisson-Boltzmann equation, which is extensively discussed—including its limitations—in [8]. Because deviations from the classic picture are found experimentally (e.g. [9]), modern conceptual works discuss in more detail solvation effects, fluctuations and ion correlation [10–14].

### 2.1.2 *Electrochemical Potential*

As an interface is charged, the work needed for a distribution of charges needs to be considered when analysing the total free enthalpy or free energy of a system. For this purpose, in charged systems, the electrochemical potential takes the role of the chemical potential.

The electrochemical potential  $\bar{\mu}_i$  is defined as the mechanical work required to bring 1 mol of ions with valency  $z$  and hence charge  $ze$  from a standard state to a specified electrical potential and concentration. Thermodynamically, it is a measure of the chemical potential that takes into account the electrostatic contributions; it is expressed as energy per mole,

$$\bar{\mu}_i = \mu_i + z_i F \Phi \quad (2.1)$$

where  $\mu_i$  is the chemical potential of species  $i$  without considering the charge,  $F$  is the Faraday constant and  $\Phi$  the local electrostatic potential. The first term of Eq. 2.1 takes into account the chemical potential of the species  $i$  (see Chap. 8 by R. Sigel for a thorough discussion on the chemical potential in relation to the formation of mixtures), while the second term includes the free enthalpy change brought by altering the potential  $\Phi$  of the phase in which the charged species is located.  $\Phi$  is also referred to as the inner potential or Galvani potential of the phase. This approach is analogous to the addition of the interface term to the chemical potential, described in detail in Chap. 4 by G. H. Findenegg.

Bringing two phases  $\alpha$  and  $\beta$  with mobile charges into contact (consider metal/salt solution as an example) will result in an equilibrium where the electrochemical potentials of the two phases will equalise in a similar fashion as the chemical potentials for uncharged systems,

$$\bar{\mu}^\alpha = \bar{\mu}^\beta \quad (2.2)$$

For simplicity, let's consider a single-valent system, for which we obtain, using Eq. 2.1,

$$\Phi^\alpha - \Phi^\beta = \frac{\mu^\beta - \mu^\alpha}{F}. \quad (2.3)$$

The result is the built-up of an electrostatic potential across the interface. The electrostatic potential difference between the two phases is the electrode potential,

$$E_{\text{cell}} = \Phi^\alpha - \Phi^\beta. \quad (2.4)$$

We need a certain reference to quantify the potential, which is an arbitrarily chosen system, for which different choices exist in the literature [15]. In analogy to the standard term in the chemical potential, to which the concentration dependence is added, we can “dump” the standard terms into a standard electrode potential  $E^0$  for each redox system. These potentials are published in the literature typically as potential differences against the standard hydrogen electrode. They can be found e.g. in the Handbook of Chemistry and Physics [16]. The potentials are usually reported as reduction potentials, and represent the tendency of a certain species to “obtain” one or more additional electrons. The higher the potential, the higher is this tendency. The standard electrode potential is therefore a quantity similar to the free enthalpy of formation of a certain species.

The electrode potential  $E_{\text{cell}}$  is actually the potential of a single electrode. When putting two of these half-cells into electrical contact, electrons can flow through an external circuit and balance the electrode potential differences which are present. At the same time, a chemical transformation occurs: one species is reduced and one is oxidised. In one of the half cells, there will thus occur oxidation, i.e. electron “loss” of the atoms or molecules, and on the other side, there will be reduction, i.e. “gain” in electrons for a certain species. As other chemical reactions generate heat or light, redox reaction can be used to generate an electrical current, and likewise, electrical current can be used to “drive” redox reactions in a certain direction. The half cell, in which oxidation occurs, is called the “anode”, and the half-cell, in which reduction occurs is the “cathode”. Note that these definitions rely on the nature of the reaction that is occurring, not on the direction of the current flow or the charge. The difference in standard free enthalpy is related to the difference in standard electrode potentials to

$$\Delta G^\circ = -zFE_{\text{cell}}^\circ. \quad (2.5)$$

If  $E_{\text{cell}}^\circ > 0$ , the process is spontaneous, as e.g. in galvanic cells, batteries or corrosion of metals. On the other hand, if  $E_{\text{cell}}^\circ < 0$ , the reverse reaction is spontaneous, as e.g. in electrolytic cells.

Moving away from the standard standard state, Eq. 2.5 keeps its validity. So, at each concentration of involved species,

$$\Delta G = -zFE_{\text{cell}}. \quad (2.6)$$

For a redox reaction of the type



the Nernst equation determines the electrode potential for an individual half-cell as

$$E = E^0 - \frac{RT}{nF} \ln \frac{[\text{Red}]^\gamma}{[\text{Ox}]^\alpha}, \quad (2.8)$$

where the activities may be approximated as concentrations in dilute solution. Here we dropped the subscript <sub>cell</sub> for convenience. Equipped with the Nernst equation, we can determine electrode potential differences, and hence free enthalpy differences from equilibrium, from tabulated standard electrode potentials, knowing activities/concentrations of dissolved species [1].

### 2.1.3 Currents Are a Measure of Reaction Rates

Electric current is the flow rate of electric charge  $q$  through a system, where  $t$  denotes the time,

$$I = \frac{dq}{dt} \quad (2.9)$$

In interface science, normalising the current in Eq. 2.9 by the interface area  $A$  is in general convenient, introducing current density  $i = I/A$ , i.e. current per unit area of electrode. The current through an interface is thus a convenient measure of the rate of electron transfer. If there is only a single electron transfer going on, the current density is directly related to the rate of the chemical reaction. It is possible to relate to the current through Faraday's law

$$I = \frac{dq}{dt} = \frac{nzF}{t} \quad (2.10)$$

to the total amount  $n$  of transformed substance, e.g. in a reaction like in Eq. 2.7. The magnitude of the current flowing at any potential depends on the kinetics of electron transfer. (Alternatively, in practise it often depends on the kinetics of transport to the interface. This case, is, however, not of interest in the understanding of the mechanistic aspects of reactions, which is why it is not considered here.)

At any electrode potential, the measured current density is given as the sum of an anodic and a cathodic partial current

$$i = i_a + i_c. \quad (2.11)$$

Here, anodic current  $i_a$  corresponds to the current from reaction in Eq. 2.7, while the cathodic current  $i_c$  corresponds to the current of the back reaction to Eq. 2.7. In equilibrium, i.e. at the potential given by the Nernst equation, no net reaction occurs, hence no net current flows and  $i_a = -i_c$ , i.e. the rate of forward and back reaction are equal.

### 2.1.4 Equilibrium Potential and Open Circuit Potential, a Mixed Potential

If we immerse a metal plate into a solution of its salt, we expect either the metal to dissolve (according to the reverse of reaction in Eq. 2.7), or salt ions to deposit as metal, according to reaction 7, until the equilibrium concentration is reached in the solution, as given by the Nernst equation, Eq. 2.8. The electrode potential that forms at the metal/electrolyte interface after immersion of the metal into solution, the so-called open circuit potential (OCP) is hence the equilibrium potential.

However, if more than one electron transfer reaction takes place at the electrode surface, the open circuit potential is a mixed potential defined by the kinetics of all simultaneous electrochemical reactions. (Candidates are, e.g. the decomposition of the solvent, e.g. through evolution of  $H_2$  or less likely  $O_2$  from water, or the reduction of  $O_2$ , as typically found in corrosion.) At OCP, the anodic and cathodic current have same magnitude but opposite directions ( $i_a = -i_c$ ), resulting in zero net current through the interface, which is not in equilibrium.

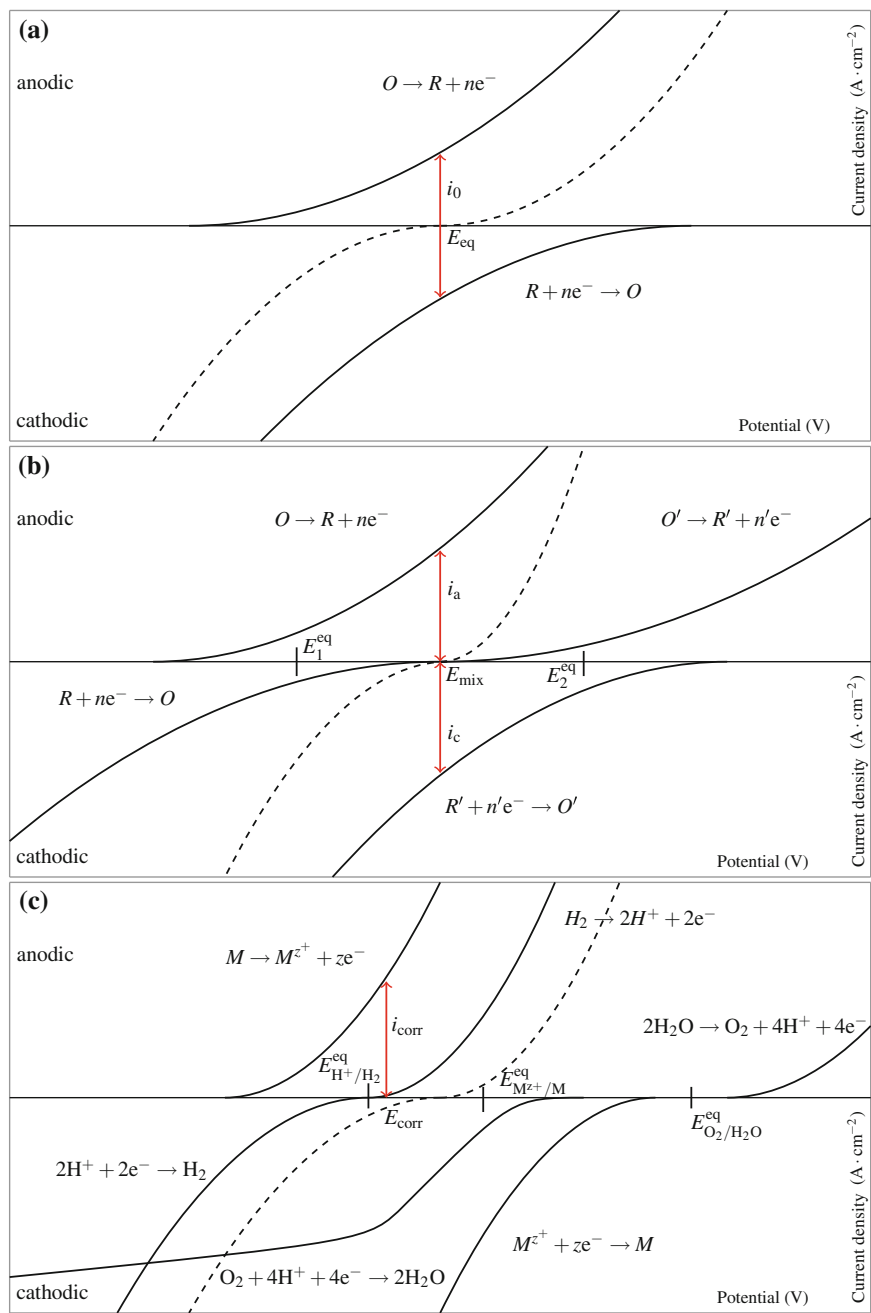
The corrosion of electrode surfaces (see also below) is explained by this theory of mixed potentials and it is based on the independence of the partial anodic and cathodic reactions. This theory states that for an electrode on which more than one electrochemical reaction takes place simultaneously [17], the measurable current-potential curves can be expressed as

$$i(E) = \sum_i |i_{a,i}(E)| - \sum_i |i_{c,i}(E)| \quad (2.12)$$

where summation is over all partial reactions.

Figure 2.2a shows the ideal situation of an electron transfer reaction, where there is an exchange current  $i_0$  at an equilibrium potential  $E_{eq}$ , that spontaneously forms when immersing an electrode into a solution.  $E_{eq}$  is a result of the contribution of the anodic and cathodic half reactions.

In Fig. 2.2b, we can observe that at open circuit conditions, the mixed potential has an intermediate value between the equilibrium potential of two reactions,  $O/R$  and  $O'/R'$ , where  $O$  stands for the oxidised and  $R$  for the reduced species. This mixed potential is determine by the kinetics of each partial reaction. (The potential dependence of the rates will be discussed in the next section.) In this case, the mixed potential corresponds to two different overpotentials,  $\eta_1$  and  $\eta_2$ , where each  $\eta$  represents the difference between applied potential  $E$  and the equilibrium (Nernst)



◀ **Fig. 2.2** Schematic partial current densities (ordinate) as function of electrode potentials (abscissa) for different situations. The *dashed line* shows the macroscopically observed current density-potential curve for the system. **a** Formation of equilibrium potential  $E_{\text{eq}}$  at an inert electrode with one redox process. **b** Formation of mixed potential  $E_{\text{mix}}$  at an inert electrode with two simultaneous redox processes, with formal equilibrium potentials  $E_1^{(\text{eq})}$  and  $E_2^{(\text{eq})}$ . **c** Formation of corrosion potential  $E_{\text{corr}}$  by simultaneous occurrence of metal dissolution, hydrogen evolution and oxygen reduction, each of them with a given equilibrium potential. The two reactions involving oxygen and hydrogen typically show some overpotential, i.e. are not fully reversible, which is why their individual exchange current densities have been put to zero

potential  $E_{\text{eq}}$ ,  $\eta = E - E_{\text{eq}}$ . Consequently, the forming potential cannot be related to either of the equilibrium potentials of the involved reactions [18].

In Fig. 2.2c, one of the partial electrode reaction is the dissolution of the electrode and the other half corresponds to the deposition on the electrode. However, deposition is not the only counter reaction to dissolution. Especially in corrosion, we typically have oxygen reduction as cathodic driving reaction for the anodic reaction. Further, in water we also have hydrogen evolution, which is also in some cases (e.g. in acidic solution) the important counter reaction. Consequently, the OCP is a corrosion potential different from an equilibrium potential, and the system dissolves at a rate given by the corrosion current  $i_{\text{corr}}$ .

### 2.1.5 Relation Between Potential and Current—Electron Transfer Reactions

The partial anodic and cathodic current densities are dependent on the concentration of the electroactive species at the site of electron transfer as typically encountered in classical chemical kinetics,

$$i_a = zF\kappa_a c_{\text{Red}} \quad i_c = -zF\kappa_c c_{\text{Ox}} \quad (2.13)$$

The rate constants  $\kappa_a$  and  $\kappa_c$  vary with the overpotential  $\eta$  in first approximation in an exponential manner as

$$\kappa_a = \kappa_{a0} \exp\left(\frac{\alpha_A n F}{RT} \eta\right) \quad \kappa_c = \kappa_{c0} \exp\left(-\frac{\alpha_C n F}{RT} \eta\right), \quad (2.14)$$

as according to the laws of thermodynamics of irreversible processes, all rates depend in first approximation exponentially on the distance of the driving force from equilibrium.  $\alpha_A$  and  $\alpha_C$  are constants between 0 and 1, known as the transfer coefficients for anodic and cathodic reactions, respectively. Typically,  $\alpha_A \approx \alpha_C \approx 0.5$ , at least on metal surfaces.



Noting the definition of the exchange current density,  $i_0 = -i_c = i_a$  at  $\eta = 0$  and rearranging we have the Butler-Volmer equation for the overall potential-dependence of the current density

$$i = i_0 \left[ \exp\left(\frac{\alpha_A z F}{RT} \eta\right) - \exp\left(-\frac{\alpha_C z F}{RT} \eta\right) \right] \quad (2.15)$$

The Butler-Volmer equation is a fundamental equation of electrode kinetics [19].

In practice, there are often-used limiting forms of Eq. 2.15. At sufficiently high positive overpotentials ( $i_a \gg i_c$ ) we find Eq. 2.16 and at high negative overpotentials ( $i_c \gg i_a$ ) Eq. 2.17,

$$\log_{10}(i) = \log_{10}(i_0) + \frac{\alpha_A z F}{\ln(10) RT} \eta \quad (2.16)$$

$$\log_{10}(-i) = \log_{10}(i_0) - \frac{\alpha_C z F}{\ln(10) RT} \eta \quad (2.17)$$

These equations present a simple method to determine exchange current density and a transfer coefficient from a linear relation and are known as Tafel equations. A useful plot is shown in idealised form in Fig. 2.3. From this plot, the OCP can be determined easily, and from the slopes of the linear region, the electron transfer coefficients  $\alpha_A$  and  $\alpha_C$  can be obtained. In the analogue plot with a linear current axis, the inverse slope around the OCP has the units of a resistance and is called the polarisation resistance  $R_p$ .

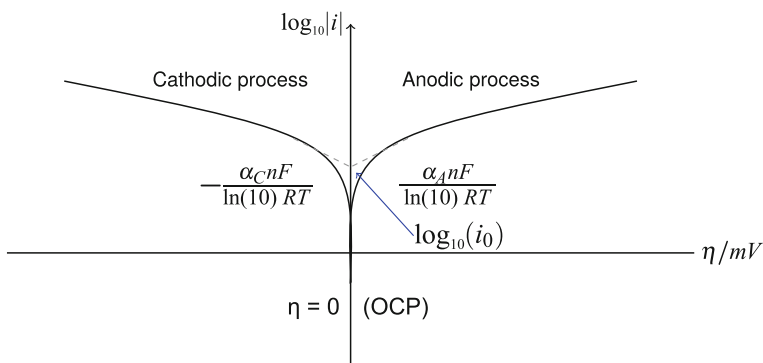


**Fig. 2.3** Schematic representation of Tafel equations. On the *left side*, the cathodic process and on the *right side* the anodic process. In this particular case, the OCP equals the equilibrium potential where  $i = 0$

Linear polarisation experiments, i.e. measurements of curves such as shown in Fig. 2.3, are widely used to determine corrosion currents. Corrosion currents can be transformed to corrosion rates, because oxidation at a certain current corresponds to a certain loss of material, though care must be taken when extrapolating. Experimentally, a sample is polarised in a range around its corrosion potential and the current response is measured. The slopes obtained in Fig. 2.3 for Eqs. 2.16 and 2.17 are called  $\beta_a$  and  $\beta_c$  for the anodic and cathodic processes, respectively. Extrapolating to the intercept of these linear regions, the exchange current density can be determined.

The corrosion or exchange current density  $i_{\text{corr}}$  can then be determined as [20]

$$i_{\text{corr}} = \frac{\beta_a \beta_c}{\ln(10) R_p (\beta_a + \beta_c)} \quad (2.18)$$

The validity of the analysis from the Tafel plot critically depends on the exponential relation between current and overpotential, i.e. more general in chemical kinetics the relation between driving force of a chemical reaction, and its rate constant. Such relations can be obtained by the application of transition state theory. The most famous example for electron transfer reaction is the Marcus theory, which represents an extension of the Franck-Condon principle to chemical reactions. (The Franck-Condon principle deals with the relaxation of the electron configuration after excitation. In electron transfer reactions, one goes one step further and transfers the electron.) The barrier for electron transfer reactions in this Marcus picture basically originates from the reorganisation of the solvation shell around the ions, because even simple ions change their charge during electron transfer, and the solvation shell needs to adapt to this change. The barrier in this theory is obtained as an intersection of two parabola (in the simplest case), which represent the interaction potential of the solvent with a central ion [21]. The central quantity in the theory is the solvent reorganisation energy,  $E_{\text{re}}$ . With a barrier from the Marcus theory, the relation between current and overpotential becomes

$$i \propto \left[ \exp\left(\frac{zF\eta}{2RT}\right) \exp\left(\frac{(zF\eta)^2}{2E_{\text{re}}RT}\right) - \exp\left(-\frac{zF\eta}{2RT}\right) \exp\left(-\frac{(zF\eta)^2}{2E_{\text{re}}RT}\right) \right], \quad (2.19)$$

which differs from the Butler-Volmer Eq. 2.15 by the presence of a term that goes with  $\eta^2$  in the exponent. For sufficiently small overpotentials, the Butler-Volmer form is obtained as limiting case, but at larger overpotentials the square term may become dominant.<sup>1</sup>

---

<sup>1</sup>An alternative approach dumps the  $\eta^2$  dependence into the transfer coefficients  $\alpha_c$  and  $\alpha_a$  by making them potential-dependent.

## 2.2 Electrochemical Methods in Corrosion Science

In Sect. 2.1.4 we saw that corrosion of metals is often essentially an electrochemical phenomenon. Hence, electrochemical techniques are used to characterise corrosion processes. This chapter introduces two important experimental techniques, electrochemical impedance spectroscopy (EIS) and scanning Kelvin probe.

### 2.2.1 Electrochemical Impedance Spectroscopy (EIS)

In EIS, the system is excited by application of a typically small alternating perturbation of the applied electrode potential, typically in a range of frequencies  $f$  between  $10^6$  and  $10^{-4}$  Hz [2]. The frequency-dependent electrical current response of the system is analysed. (An inverse variant exists, in which an alternating current is forced upon a system, and the electrode potential response is analysed. This variant shall not be discussed here.) The measured impedance can be given as a complex number, with a modulus, and a phase shift between applied potential and response current. In many cases, the frequency-dependent impedance can be described by a combination of electrical circuit elements, the so-called equivalent circuit. Therefore, the impedance of standard passive electrical circuit elements shall shortly be defined, before discussing electrochemical applications [22].

Ohm's law describes the proportionality between applied voltage  $U$ , and flowing current  $I$ , with resistance  $R$  as constant of proportionality,

$$I = \frac{1}{R} U. \quad (2.20)$$

For Ohmic conductors, this equation is valid also if an alternating voltage  $U(t)$ , e.g. with sinusoidal modulation with time  $t$ , is applied. If a sinusoidal voltage with a certain frequency  $f$  is applied, the corresponding alternating current has a certain amplitude and a phase shift  $\phi$  with respect to its exciting current. The resistance in this situation is called the impedance  $Z$ ,

$$Z = \frac{U(t)}{I(t)} = \frac{U_0 \sin(\omega t)}{I_0 \sin(\omega t + \phi)}, \quad (2.21)$$

with angular frequency  $\omega = 2\pi f$ .

If an electrical circuit consists only of a resistor, the phase shift between applied voltage and response current is zero. However, replacing the resistor with a capacitor or an inductor causes a phase shift of the impedance as schematically depicted in Fig. 2.4. Most electrochemical systems analysed by EIS can in first approximation be described by a combination of capacitors and resistors, where the so-called Randles circuit, depicted in Fig. 2.5, is the most useful circuit.

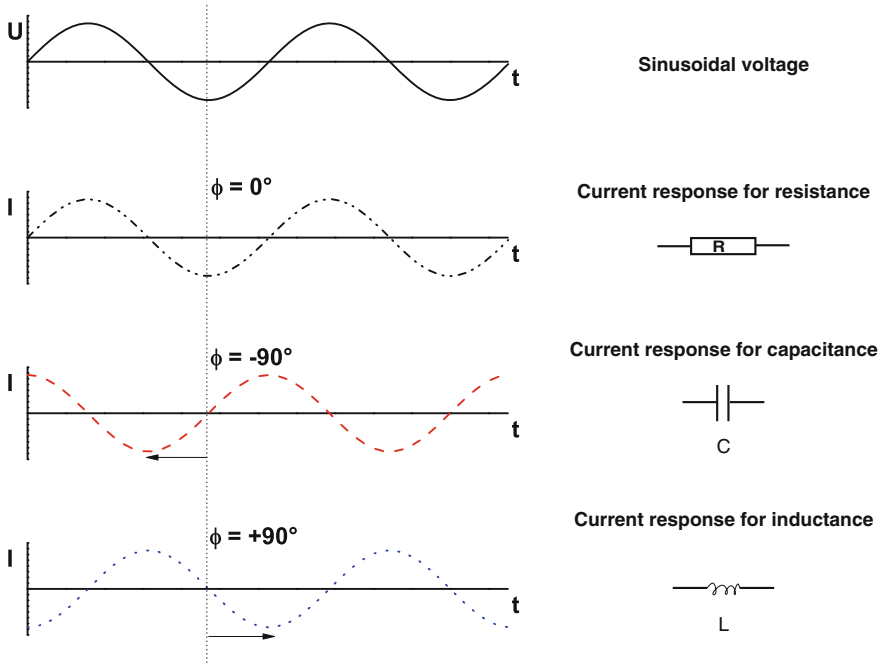


**Fig. 2.4** Schematic depiction of applied sinusoidal voltage and the corresponding current responses in the case of a resistor, capacitor and inductor

As often done in spectroscopy (see also Chap. 14 by A. Erbe et al.), a complex plane representation of the voltage can be used, in which

$$U(t) = U_0 e^{i\omega t}, \quad (2.22)$$

with  $i = \sqrt{-1}$ . Likewise,

$$I(t) = I_0 e^{i(\omega t - \phi)}, \quad (2.23)$$

which allows for a simplified description of the ratio in Eq. 2.21 as

$$Z = \frac{U_0 e^{i\omega t}}{I_0 e^{i(\omega t - \phi)}} = |Z| e^{i\phi} = |Z| [\cos(\phi) + i \sin(\phi)], \quad (2.24)$$

where  $|Z| = U_0/I_0$ . To analyse and interpret complex impedance measurements, a graphical depiction of the resulting spectrum is extremely useful. Two frequently used plots are Nyquist plots and Bode plots, depicted in Fig. 2.5 for the simple circuit elements. In the Nyquist plot, the real part of the impedance  $\text{Re}(Z)$  is drawn at the horizontal axis and the imaginary part  $\text{IM}(Z)$  at the vertical axis of a Cartesian coordinate system. The disadvantage of this plot is that the frequencies are not

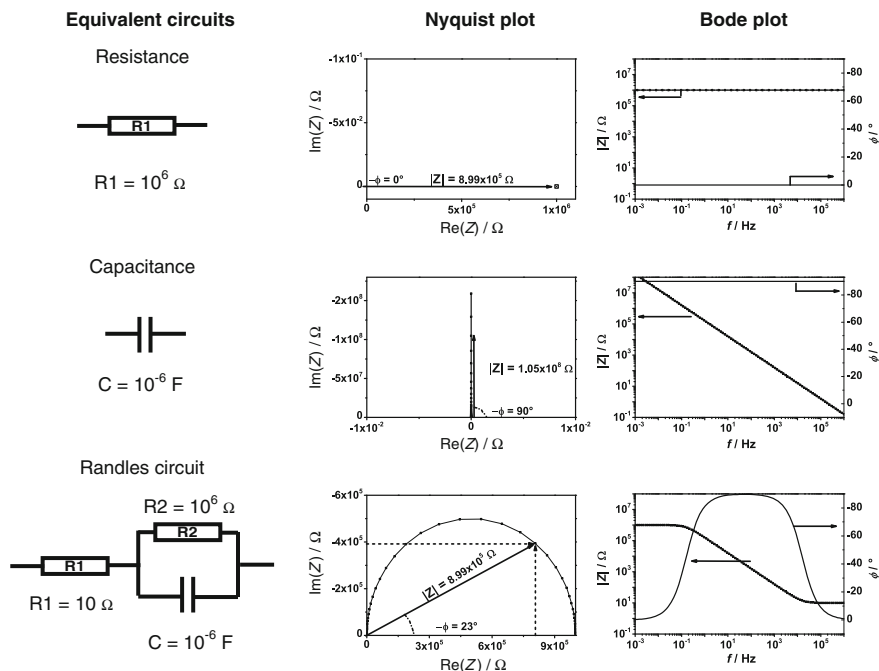


**Fig. 2.5** Comparison of Nyquist and Bode plots for the respective to the equivalent circuits

directly accessible. This disadvantage is circumvented by using the Bode plot, where the modulus of impedance and the phase shift are plotted as a function of frequency. Figure 2.5 gives an overview of the Nyquist and Bode plots obtained in accordance to the electrical circuits. A further variant is the so-called Cole-Cole plot, where  $\text{Re}(Z^{-1})\omega^{-1}$  is plotted against  $-\text{Im}(Z^{-1})\omega^{-1}$ . In this case the axes have the unit of capacitance, and hence a capacitance can directly be obtained from the plots.

All equations mentioned previously are in first approximation also valid for an electrochemical system. The voltage  $U$  is replaced by the electrode potential  $E$  and current  $I$  is replaced by the current density  $i$ . The analogy to electrical circuit elements works only if a linear relationship between potential and current density exists. As discussed in Sect. 2.1.5, this relationship is in general not linear. The actual exponential relation can be approximated by a linear relation only in a rather small electrode potential range. Thus, there will be an error in the measurement due to the fact that the current will not be sinusoidal any more. But in a very narrow region around a certain applied potential or OCP, typically  $\pm 10$  mV (depending on application between 5 mV and 30 mV root mean square) the relationship between potential and current density is approximated as linear. Several possible applications exist in electrochemistry, e.g. in-depth analysis of reaction rates for corrosion phenomena, or an analysis of the corrosion resistance and water uptake of a coating,

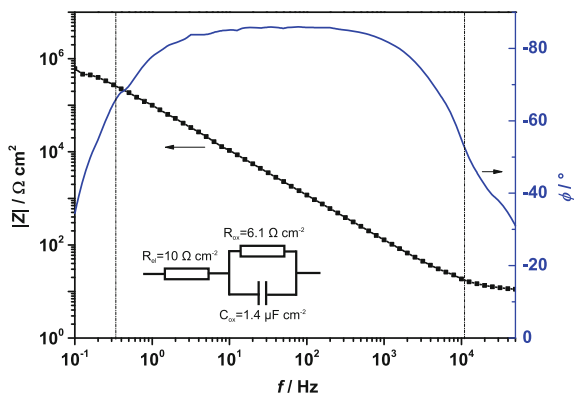
as will be shown in Sect. 2.4.2. More advanced measurement schemes make use of the non-linearity to access detailed information on electron transfer [23].

The advantage of EIS compared to other electrochemical techniques is the fact that one can get a relaxation picture of electrochemical systems under quasi steady state conditions. The reason is that electrochemical reactions especially in corrosion science involve several electrical and ionic processes at the interface between substrate and electrolyte and that every reaction has its own relaxation time. While the rearrangement of water molecules or solvated ions in an electrolyte under potential control is an extremely fast reaction (e.g. because of the Grotthuss mechanism) with relaxation times in the range of 1 ms to 10 s, the diffusion controlled dissolution of a metal, which involves diffusion along the metal electrolyte interface, is a much slower process. Hence, the resistance of an electrolyte can be measured at high frequencies and the dissolution phenomena at lower frequencies.

Figure 2.6 shows a typical impedance spectrum of aluminium recorded in an acetate buffer at OCP. The Randles circuit introduced in Fig. 2.5 is used to extract data about the aluminium oxide. The circuit consists of a resistance simulating the electrolyte resistance  $R_{el}$ , and an RC element with  $R_{ox}$  as the oxide resistance and  $C_{ox}$  as the oxide capacitance. In the high frequency region, the electrolyte resistance dominates the spectrum. In the mid-frequency region,  $|Z|$  increases due to the fact that more and more the capacitive character of the oxide is contributing to the impedance, as it can be also seen in the phase shift (note, that the current flow through a capacitor is frequency dependent—while the capacitor is short circuited at high frequencies, at lower frequencies it acts as an insulator). At lower frequencies the current flows completely along the resistances  $R_{el}$  and  $R_{ox}$  and the oxide resistance is the dominating factor. More detailed information on characterizing aluminium oxides and kinetic of growth with electrochemical techniques can be found in [24] and in the references cited therein.

Using a Randles circuit is often the starting point for building an equivalent circuit for describing and simulating more complex phenomena, like coatings. We shall return to this description and its application to protecting organic coatings in

**Fig. 2.6** Electrochemical impedance spectrum of aluminium in a 0.1 M acetate buffer pH = 6 and the values received by fitting the curve with a Randles circuit



Sect. 2.4.2. Nevertheless, the usage of equivalent circuits has its limits, and an ongoing discussion concerns the validity of separating capacitive from Faradaic currents [25]. Further in-depth discussion on the use and validity of equivalent circuits can be found elsewhere [26, 27].

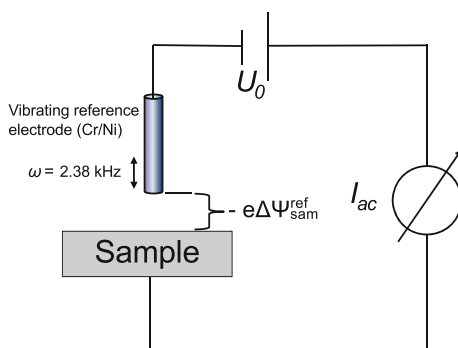
### 2.2.2 The Scanning Kelvin Probe (SKP)

While it is rather straightforward to obtain the electrode potential of a metal if the metal is immersed in electrolyte, many practical problems involve corrosion of samples in contact with an atmosphere. Electrode potentials, and to a certain extent also currents, can be obtained under atmospheric conditions by Kelvin probe measurements. Consequently, the scanning Kelvin probe (SKP) has been a valuable and versatile tool for studying corrosion problems of metals under thin electrolyte layers [28–33], and at buried interfaces beneath organic coatings [34, 35]. In principle, the Kelvin probe measures the work function [36] or, for non metallic surfaces, the surface potential of a sample. The work function itself is extremely sensitive to changes in the surface conditions and is directly influenced by e.g. adsorbed layers, charges and functional groups at the surface, surface and bulk contaminations, and for semiconducting oxides structure, doping and even imperfections [37–42].

The SKP permits a non-destructive in situ measurement of electrode potentials at buried polymer/metal interfaces with certain spatial resolution. The principle of the Kelvin probe is based on the vibrating capacitor method (see Fig. 2.7): a needle (that acts as a reference and is often referred to as “the probe”) consisting of an inert corrosion-resistant metal, like Ni/Cr (80/20 wt%) alloy, is positioned approximately 50–100  $\mu\text{m}$  close to the surface of the sample [43–46].

As soon as the needle and the sample are brought into electrical contact, the equilibration of the Fermi levels within the two metals will result in the formation of

**Fig. 2.7** Working principle of the Kelvin probe



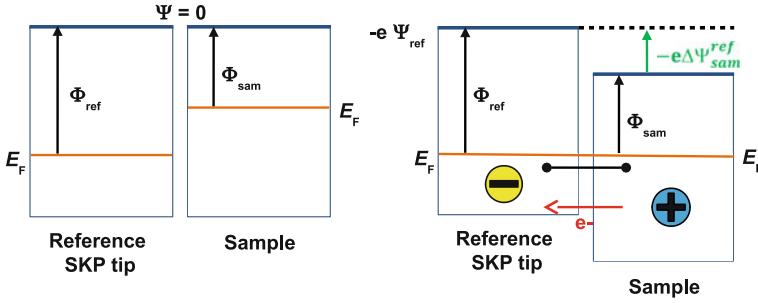


**Fig. 2.8** Illustration of the Fermi level alignment of the the SKP tip and the sample. Corresponding measured Volta potential difference  $\Delta\Psi_{sample}^{ref}$

a positive charge on the surface of one and a negative charge on the surface of the other metal. Thus, the needle and the sample form a capacitor and the charging of the sample with respect to the probe leads to a Volta potential difference  $\Delta\Psi_{sample}^{ref}$  between the two metals (Fig. 2.8). By vibrating the needle, a current will be induced. If an external bias is applied between sample and the needle in a way that this current is compensated, surfaces will be uncharged again, the capacitance will go to zero and the original state will be obtained. Under such conditions the external bias voltage is identical to the Volta potential difference.

The work function describes the energy required to liberate an electron from an electrode's Fermi level to the vacuum level. For a metal in vacuum, the electron only has to pass the metal surface during this transfer. However, if the metal is covered by other phases, such as an aqueous electrolyte, a polymer layer or even a coated metal affected by wet deadhesion, the electron needs to pass additional interfaces. Thus, the measured Volta potential difference is strongly affected by additional potential differences across these interfaces. As a consequence, the Volta potential difference measured by the SKP is determined by the interfacial electrode potential. Therefore, changes within the interfacial structure can be detected. Depending on the different interfaces involved in the measurement, the measured Volta potential difference  $\Delta\Psi_{sample}^{ref}$  can be correlated to the corrosion potential of the underlying metal  $E_{corr}$ . Practically the following cases can be distinguished. Metal surface covered by a liquid phase [47]:

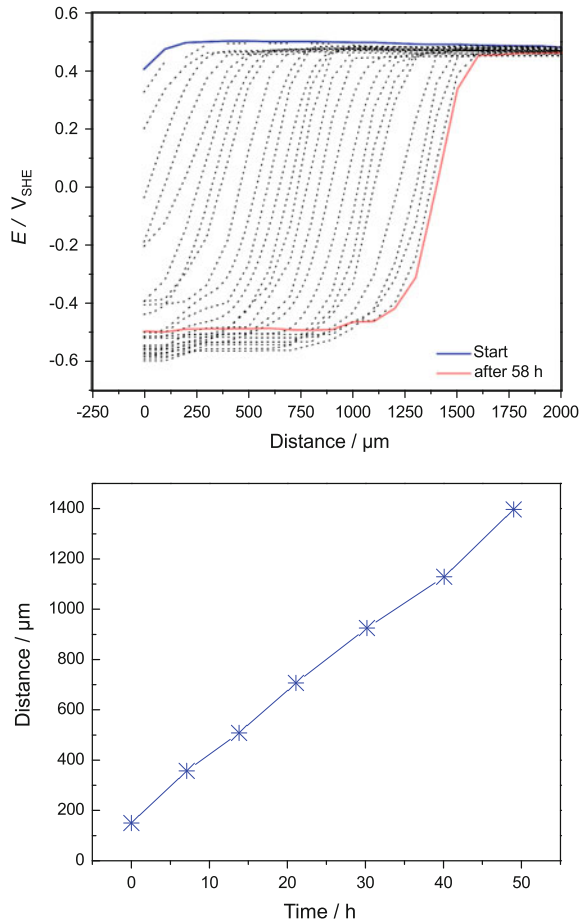
$$E_{corr} = \left( \frac{W_{ref}}{F} - \chi_{El} - E_{1/2}^{Ref} \right) + \Delta\Psi_{sample}^{ref} \quad (2.25)$$

Metal surface covered polymers with negligible dipole potentials [47]:

$$E_{corr} = \left( \frac{W_{ref}}{F} - \chi_{Pol} - E_{1/2}^{Ref} \right) + \Delta\Psi_{sample}^{ref} \quad (2.26)$$



**Fig. 2.9** *Top* Typical potential distribution of a polymer covered zinc substrate (as model for galvanised steel, i.e. steel covered with a metallic zinc layer) in humid air for different delamination times detected with the SKP (electrolyte in the defect: 1 M KCl). *Bottom* Time dependence of the delamination front position



Additional liquid phase between the metal and the coating (during deadhesion) [47]:

$$E_{\text{corr}} = \left( \frac{W_{\text{ref}}}{F} - \chi_{\text{Pol}} - E_{1/2}^{\text{Ref}} \right) + \Delta\psi_{\text{sample}}^{\text{ref}} + \Delta\Phi_{\text{D}} \quad (2.27)$$

where  $W_{\text{ref}}$ ,  $\chi_{\text{El}}$ ,  $E_{1/2}^{\text{Ref}}$ ,  $\chi_{\text{Pol}}$ ,  $\Delta\Phi_{\text{D}}$  and  $F$  denote the work function of the reference (probe/needle), the surface dipole potential of the electrolyte, the half-cell potential of the reference (probe/needle), the surface dipole potential of the polymer surface, the Donnan potential of the polymer and the Faraday constant, respectively. These equations show two advantages of the SKP: (1) The measured Volta potential difference  $\Delta\psi_{\text{sample}}^{\text{ref}}$  is related to the corrosion potential in a linear manner; (2) The electrode potential of the buried interface can be determined across a dielectric medium of infinite resistance. Due to the linear nature of the equations, a calibration

constant is required in order to calculate the electrode or corrosion potential from a Volta potential difference measurement. In practice, this constant can be obtained for aqueous electrolytes simply by measuring the  $\Delta\psi_{\text{sample}}^{\text{ref}}$  between the needle used for the measurements and a metal electrode (as sample) which is exposed to an electrolyte containing the metal cation in a defined concentration. Commonly, the calibration is performed against a Cu/CuSO<sub>4</sub> electrode [46].

In corrosion science, SKP has been used to study delamination kinetics and mechanisms of organically coated metals [30, 43–45, 48–50], also with control of surface chemistry [51], or morphology [52, 53]. In the following, an example for cathodic delamination will be given. In the presence of moisture and oxygen, the electrode potential of the buried coating/metal interface is changing in a well-defined manner with increasing distance from a defect. A defect can be an artificial scrape or defect, a cut edge, or a coating defect like a blister. For steel (including galvanized steel that is covered with a zinc layer), basically two potential levels characterise the SKP profiles measured during delamination. The potential of the defect, and of the potential of the intact coated area. In most cases, the potential close to the defect has a very negative value (pointing to cathodic processes), whereas far away from the defect predominantly positive potentials are observed (see Fig. 2.9). The progress of cathodic delamination is reflected by the lateral displacement of steep increase within the repeatedly measured potential profiles. The order of the delamination kinetics can be seen if the delamination front position is plotted against the exposure time: A linear relation suggests that the process of delamination is reaction controlled, whilst a hyperbolic (or square-root) relation suggests that the interfacial ion mobility is rate-determining. We will return to the discussion of the actual failure mechanisms in Sect. 2.4.3, after briefly looking at the chemical composition of the polymer coatings, which are frequently used in corrosion protection.

## 2.3 Types of Binder Resins for Passivating Organic Coatings

From the discussion in Sects. 2.1.4 and 2.1.5, it is clear that simple ways of protecting a metal against corrosion are to reduce the active area, to reduce the access of oxygen and finally also to reduce the access of water to the metal. Such reduction in accessibility is reached by barrier coatings, and organic coatings often are used as such. If the coating properly wets the substrate surface and shows good adhesion even in the presence of water and electrolyte, then sufficient protection can be achieved. To create that effect, the choice of an appropriate binder resin is crucial. These binder resins are generally organic polymers which can be classified with respect to their chemical structure. From an industrial point of view, the most important resins are hereby polymers made from epoxides, polyurethanes, polyesters, melamine formaldehyde resins, polyacrylates and phenolic polymers. The

chemical background and the properties of these classes are described in more detail in the following paragraphs [54].

### 2.3.1 Epoxy Based Coatings

Resins for epoxy coatings are derived from compounds that contain one or more epoxy groups. These are derivatives of the three-membered, heterocyclic oxirane ring, which is also called ethylene oxide, epoxy ethane, 1,2-epoxide or oxacyclopropane. The methyloxirane form is also known as glycidyl group. Due to its high ring strain, the epoxy group is highly reactive and can therefore be converted with many different functional groups [55, 56].

The most basic and most frequently used epoxy resin is prepared by the reaction of bisphenol A with two moles of epichlorohydrine in alkaline medium to form the diglycidyl ether of Bisphenol A (DGEBA) according to Fig. 2.10. After reaction with the hydroxyl group, the epoxy ring is reformed by elimination of HCl, and is then available for further reactions. If it is converted again, a secondary hydroxy group is created. By varying the ratio of Bisphenol A to epichlorohydrine, a broad variety in molecular weight can be obtained. Since the molecular weight of DGEBA is only 340 g/mol, it is available in liquid state. With a mean molecular weight of 1000 g/mol, a polymer made from the same reactants is solid at room temperature. On the one hand, low molecular weight molecules can be used to obtain thick coatings, because there is only little solvent that needs to evaporate. On the other hand, high molecular weight epoxy polymers have a higher strength, but must be dissolved in organic solvent to render them utilisable for manufacturing and the application processes [55, 56].

In most cases, epoxy polymers are cross-linked to improve the mechanical properties and the heat resistance of the coating. This process implies the usage of hardeners, which are agents that can react with the secondary hydroxyl group

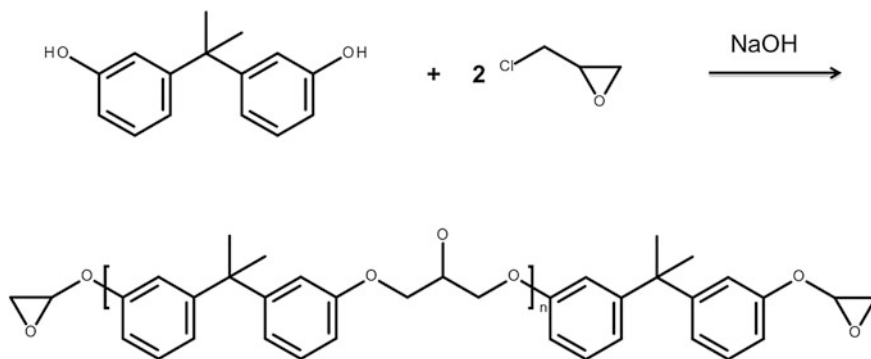
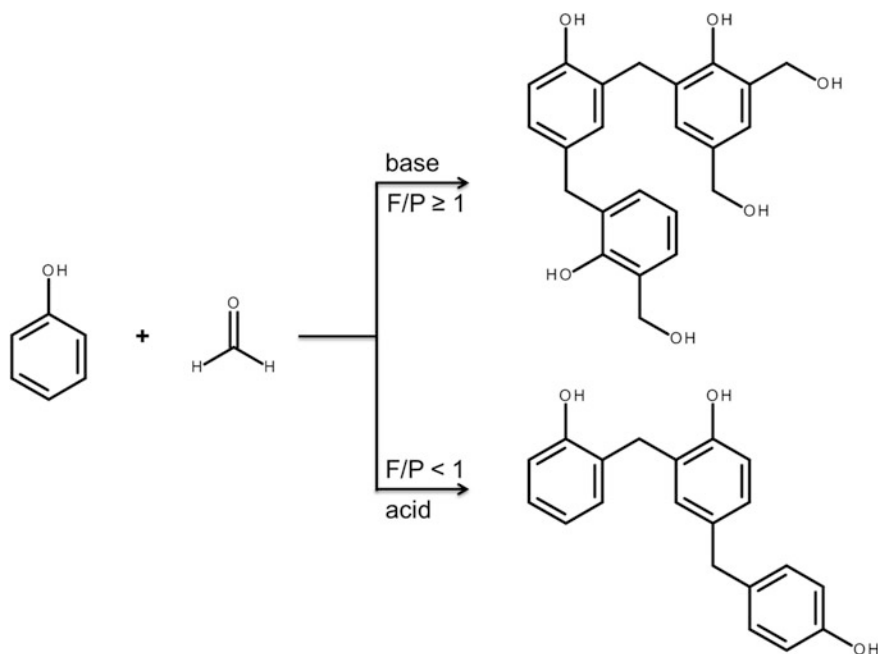


Fig. 2.10 Reaction of Bisphenol A with epichlorohydrine

and/or with the terminal epoxy groups. Examples of substances that can react with epoxy groups are amines, acids and acid anhydrides, alcohols and mercaptans. Furthermore, instead of reaction with the hardener, the terminal epoxy groups can also be used for further modification of the binder resin to tune the properties in a desired way [55, 56].

### 2.3.2 Phenol Formaldehyde Resins

Another binder resin can be obtained by the condensation reaction of phenol, or substituted phenols, with aldehydes, e.g. phenol (P) with formaldehyde (F). Products are classified as novolacs or resols. The first class is synthesized under alkaline pH conditions with an excess of F. The latter is produced in acidic medium with an excess of P. Both reactions are highly exothermic. The different architecture of the hereby achieved products is shown in Fig. 2.11. If the molar ratio of F and P is equal to one or higher (as for resol), every phenol is theoretically linked to another phenol by a methylene bridge and there are also additional aldehyde moieties available that can be used for later hardening. Having a lower amount of F, novolac only hardens with addition of a cross-linking agent. Phenol formaldehyde



**Fig. 2.11** Reaction of phenol and formaldehyde to resol and novolac

resin based coatings are utilized for high temperature applications and very humid and aggressive environments [55, 56].

### 2.3.3 Polyurethane Resins

Polyurethanes are materials which are traditionally formed by reaction of a compound containing two or more isocyanate groups with a polyol to form urethane bonds as shown in Fig. 2.12. The broad applicability of polyurethane coatings is due to the versatility in selection of monomeric materials from a huge list of diisocyanates, like hexamethylene diisocyanate, toluene diisocyanate or isophorone diisocyanate, and diols, macrodiols or polyols. Cross-linked polyurethanes provide hard and dense coatings with a very good chemical and moisture resistance and are the most versatile group of polymers in industry [55, 56].

### 2.3.4 Polyacrylate Resins

Polyacrylate resins are synthesized from ethylenically unsaturated monomers which are esterified derivatives from (meth)acrylic acid. These monomers can be equipped either hydrophobic or hydrophilic and can insert special functionalities into the resin. The product is usually obtained by emulsion or solution polymerisation started by initiators that dissociate into free radicals under elevated temperature. In a chain reaction, an acrylic polymer is build-up in a very short time according to Fig. 2.13 [55, 56].

Commercially available polyacrylic resins are based on monomers like ethyl acrylate, ethyl acetate, n-butyl acrylate, methyl methacrylate, vinyl acetate, acrylic

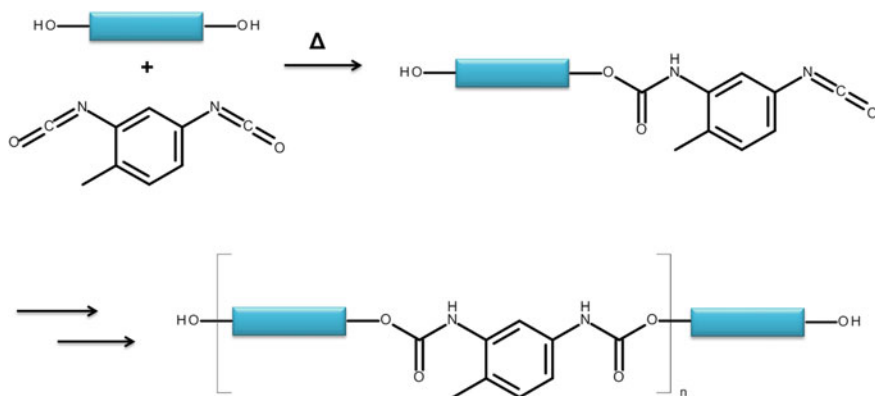


**Fig. 2.12** Formation reaction of polyurethane from toluene diisocyanate and a macrodiol

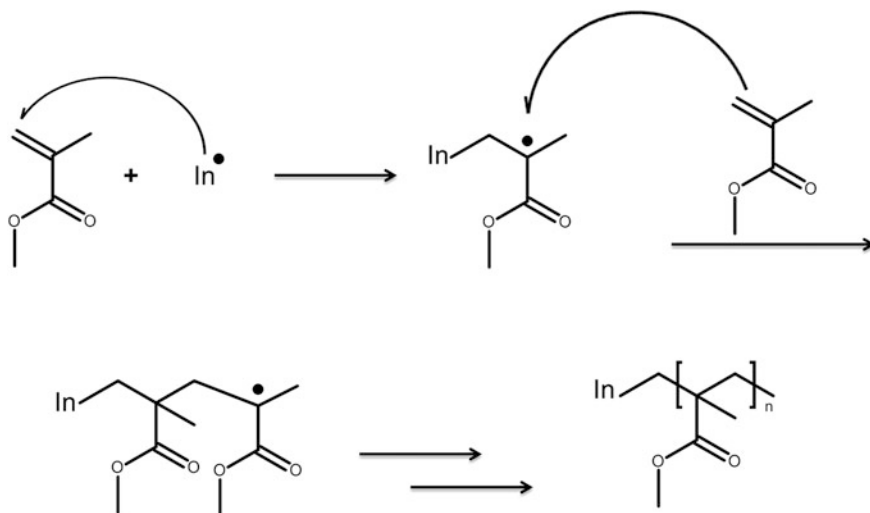


**Fig. 2.13** Radical polymerisation of methyl methacrylate as example for the build-up of a polyacrylate

acid and other derivatives thereof. Furthermore, multifunctional acrylic monomers such as ethylene glycol dimethacrylate, trimethylolpropane trimethacrylate, 1,4-butanediol dimethacrylate or neopentyl glycol dimethacrylate can be used in small amounts to act as cross-linkers. Usually, high molecular weight polymers can be created by this reaction. Chain transfer agents like mercaptans can be incorporated to control the formation of long chains [55, 56].

### 2.3.5 Polyester Resins

Polyesters resins are made from di- or polyols and dicarbonic acids or anhydrides via a step-wise condensation reaction according to Fig. 2.14. This procedure involves a long reaction time because the produced water has to be constantly distilled from the often high viscous reaction mixture. Appropriate monomers are phthalic anhydride, isophthalic anhydride, terephthalic anhydride, trimellithic anhydride, adipic acid, maleic anhydride, fumaric acid, glycol, 1,4-butane diol, trimethylolpropane, neopentyl glycol and many other acids or alcohols [55, 56].

Alkyd resins represent a special class of polyester resins, which contain mainly glycerin and different fatty acids combined with other dicarbonic acids and alcohols or diols. Hydroxyl functional oligo- or polyesters can also be used as building block e.g. for the synthesis of polyurethane resins. Polyesters with unsaturated double bonds can be used for later cross-linking with acrylic monomers [55, 56].

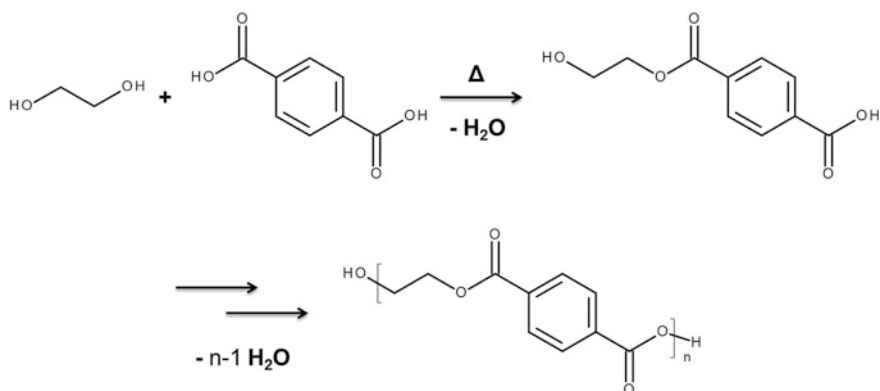


**Fig. 2.14** Condensation reaction of ethyl glycol and terephthalic acid as example for polyester formation

Overall, polyesters can be designed with a broad variety of different properties and can therefore be used in various coating systems [55, 56].

### 2.3.6 Melamine Formaldehyde Resins

An important class of binders is obtained by the reaction of melamine with formaldehyde and further etherification to obtain multifunctional hardeners according to Fig. 2.15. Depending on the amount and character of modification, these show higher or lower reactivity with alcohols. A faster reaction at lower

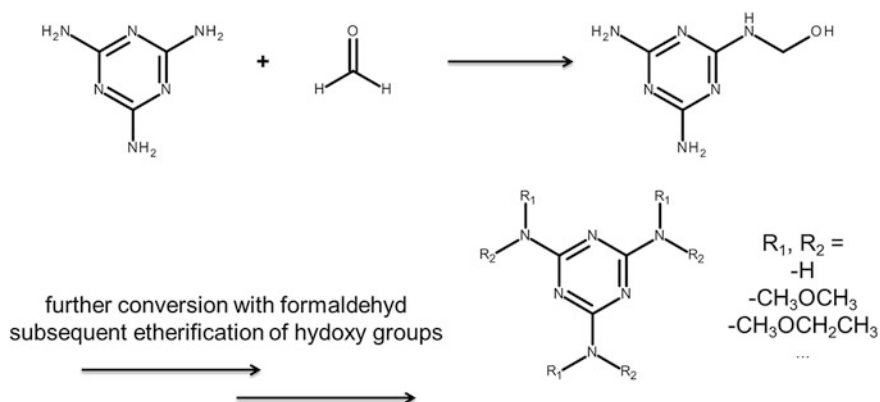


**Fig. 2.15** Reaction of melamine and formaldehyde to form differently modified melamine formaldehyde resins

temperatures is usually achieved with more N-H-groups that are still available and shorter carbon chains within the ether segments [55, 56].

## 2.4 Coating Performance and Failure

### 2.4.1 *Multilayer Coatings Are Applied in Real Coating Applications*

In the automotive sector, multi-layer coatings are applied to fulfil corrosion protection standards [57]. Moreover, the whole spectrum of different and sometimes contrary properties desired for automotive coatings can be achieved and balanced only by the interplay of several layers. Usually, the top layer is represented by the clear coat. It provides not only the scratch resistance and the gloss, but protects also from all outer influences like humidity, sunlight, chemicals and natural compounds like bird droppings or tree resins. The colourful appearance and the metallic effects are delivered by the second layer from top, the base coat. Beneath that more “superficial” job, it provides adhesion between the upper and lower layer. The second-named is the filler that serves as a kind of protective shield against damage from stone chips. This flexible and thick layer also smooths the surface in preparation for the decorative layers and, to some content, provides protection against corrosion, owing to its barrier properties. The task of protection is mainly fulfilled by the lowest layer of a standard automotive coating: the cathodic electrodeposition coating (e-coat). Whereas all other layers are applied via spray application, this one is precipitated by an electrochemical approach. The car body is connected as cathode and the positively charged paint particles are attracted, thereby leading to a good surface coverage. Together with the pre-treatment and galvanization layer of the steel, the e-coat gives an appropriate protection against corrosion. The stack of these four layers is shown in Fig. 2.16, applied according to a standard procedure. Modern processes try to get rid of single layers to save time, money and energy. Of course, the same good overall properties should be maintained [54].

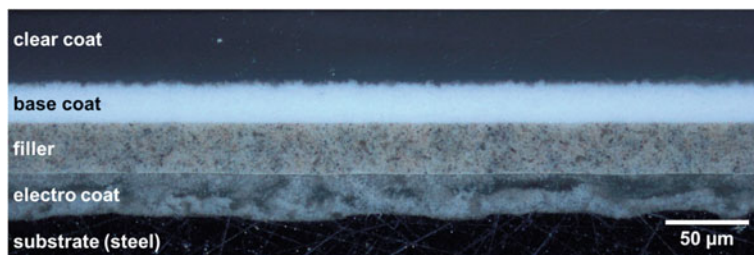


**Fig. 2.16** Microscopic picture of a crosscut of a standard build-up of an automotive coating



For industrial coatings, the focus is a bit more on the side of protection than of decoration. For such applications, the clear coat and base coat functions are combined within a topcoat layer. Below that, the so called primer is responsible for corrosion resistance and adhesion to the metal. This layer contains inhibitor pigments to actively inhibit the corrosion at a defect.

### 2.4.2 Accessing Coating Barrier Property with EIS

All organic coatings are to some extent permeable to water and corrosive ions. The driving forces for water permeation are: (1) a concentration gradient (e.g. during immersion), (2) osmosis (e.g. from impurities at a coating/coating interface) or (3) capillary forces (e.g. defects in the coating due to inadequate curing or improper solvent evaporation). Corrosion underneath organic coatings could be basically classified in two categories: (1) Delamination and blistering of the coating due to clustering of water at the interface leading to wet deadhesion or osmotic blistering and (2) delamination caused by specific corrosion mechanisms like cathodic or anodic delamination. Often, the formation of blisters is the starting point for cathodic or anodic delamination processes. Therefore, it is important to study the barrier properties of organic coatings towards water and ions.

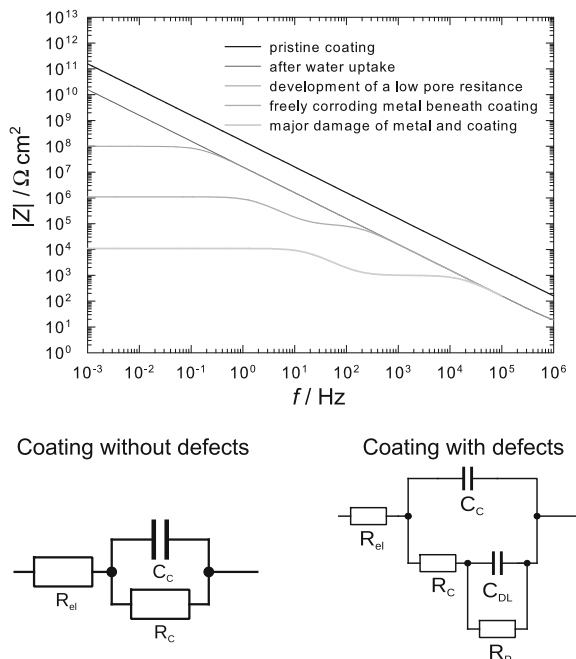
EIS was already introduced in Sect. 2.2.1 as a powerful tool for the electrochemical characterisation of interfaces. The final purpose of the EIS characterisation of protecting organic coatings is to obtain information about system properties, such as the presence of defects, reactivity of the interface, adhesion, and barrier properties to water. Practically speaking, EIS can quantitatively measure both the resistance of the organic coating to aqueous and/or ionic transport, and capacitances in the electrochemical cell. In this context, a resistance implies a current flow, and hence the presence of electron transfer reactions, like corrosion. Organic coatings deteriorate with time during exposure to an electrolyte. Deterioration can be monitored e.g. as a change in the capacitance of a coating.

During exposure to corrosive electrolytes, metals covered with organic coatings pass basically through four different stages of deterioration [47, 49, 50, 58]:

- Water uptake within the organic coating.
- Corrosion underneath the coating without any defect in the coating itself.
- Partially damaged coating with cracks, defects or pores reaching the metal surface.
- Partially damaged coating with corrosive undermining of the coating.

These physical and chemical processes are usually quantified by means of equivalent circuits, see also Sect. 2.2.1. Each element of the equivalent circuit depicts one constituent of the specimen that is in contact to the electrolyte [59–61]. Schematic impedance spectra with the corresponding equivalent circuits for the different stages of deterioration of metal coated with polymers exposed to corrosive electrolytes are illustrated in Fig. 2.17. The parameters in the equivalent circuits are:

**Fig. 2.17** Bode plots of typical impedance response of coatings with and without defects and the corresponding equivalent circuits



- $R_{el}$ : Uncompensated electrolyte resistance of the electrolyte between the working and reference electrode, which is usually very low.
- $C_C$ : The coating capacitance changes e.g. due to water uptake or swelling.
- $R_C$ : The pore or coating resistance changes during exposure due to the penetration of the electrolyte into pores and defects of the coating.
- $C_{DL}$ : Interfacial capacitance at the metal/electrolyte interface.
- $R_P$ : Polarization resistance of the metal surface that is in contact with ionically conducting paths through the coating.

The two quantities that dominate the impedance during the initial stages of immersion are usually  $C_C$  and  $R_C$ : Typically,  $C_C \sim 10 \text{ nF cm}^{-2}$  of an undamaged pristine coating (e.g. for automotive or coil coating applications) with good barrier properties. This capacitance corresponds to a modulus of the impedance at 0.1 Hz of  $10^9 \Omega \text{ cm}^2$ .<sup>2</sup> Upon immersion,  $R_C$  is exceedingly high ( $10^{12} \Omega \text{ cm}^2$  or even more), which leads to a nearly ideal capacitive response in the impedance. Capacitance decreases over orders of magnitude with increasing exposure time, leading to a horizontal plateau in the Bode plot at low frequencies. The pore resistance of a coating is directly influenced by many parameters like the crosslinking density or pigment to volume ratio, amongst others.

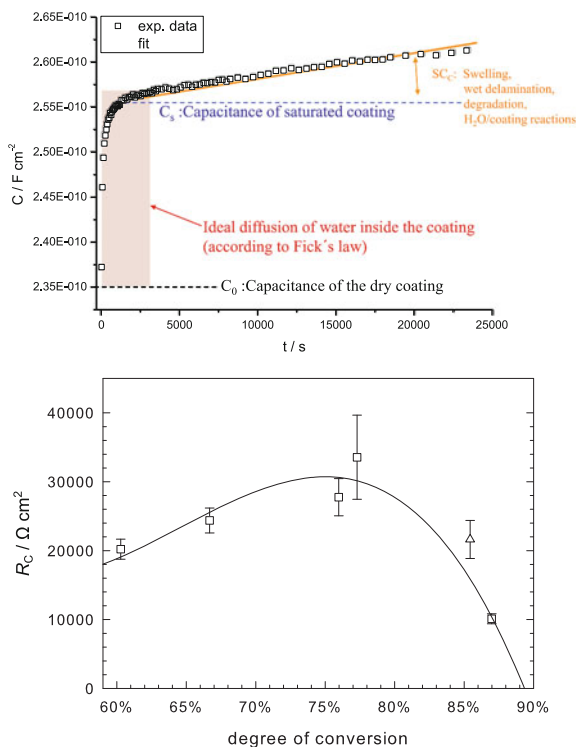
<sup>2</sup>In the units here, the electrode area dependence has been removed, which is critical for comparison of different coatings. As  $C \propto A$ , a comparison of  $C/A$  in  $\text{F m}^{-2}$  is independent of electrode area. Likewise, as  $R \propto 1/A$ ,  $RA$  with units of  $\Omega \text{ m}^2$  is independent of electrode area.

One example how structural parameters of a coating can influence the barrier properties is shown in Fig. 2.18 [49]: The pore resistance of a pigment free UV-curable chlorinated polyester changes significantly with immersion time and degree of conversion (which is proportional to the cross-link density). Due to the formation of the polymer network  $R_C$  rises with increasing degree of conversion until the on-going polymerisation of the coating leads to internal stress within the coating [49]. Consequently the coating resistance drops for higher degree of conversion.

The water uptake changes the dielectric constant of the polymer and therefore the impedance and the capacitance of the coating:  $C_C = \epsilon \epsilon_0 A / d$  (with  $\epsilon$ : dielectric constant of the coating,  $\epsilon_0 = 8.8510^{-14} \text{ F cm}^{-1}$ ,  $A$  area of exposure,  $d$  thickness of the coating). At ambient conditions, the dielectric constant of a coating ranges between 2 and 8, whereas that of water is nearly 80. As consequence, the water uptake by the coating will lead to a significant increase in the effective dielectric constant of the coating and therefore in  $C_C$ .

A common approach for evaluating impedance spectra during water uptake is the determination of the diffusion coefficient  $D$  of water diffusion through the coating based on Fick's second law by fitting the development of the coating capacitance  $C_C$  values with time (see Fig. 2.18) [59, 62]. Theoretically, for ideal

**Fig. 2.18** *Top* Typical time evolution of a coating capacitance upon immersion to 5 % NaCl. *Bottom* Dependence of coating resistance ( $R_C$ ) of the differently UV-cured polyester acrylate layers after 1 h of exposure to the electrolyte (based on [49])



coatings plotted capacitances show an exponential increase in the initial stage of water uptake [Fickian (case-I) diffusion of water into the coating] and then result in a saturation plateau (eventually followed by another raise of inhomogeneous water accumulation due to polymer breakdown). However, water uptake curves measured on real polymeric systems (e-coating, coil coating, complete OEM lacquers, powder coatings, primer layers,) almost never show this ideal behaviour. These films tend to undergo swelling, degradation or other transport processes during longer exposure times to an electrolyte. As a result, the polymer capacitance does not reach a constant value after water saturation with time, but shows an additional increase (or decrease if the coating just undergoes a swelling transition) in the capacitance (see Fig. 2.18). Empirically, this additional increase typically shows often a linear behaviour. To quantify these influences and to improve the accuracy of the calculated diffusion coefficients, this increase can be mathematically compensated by combining Fickian Diffusion and case-II-sorption, e.g. by adding a slope coefficient to capacitance values [59]. This model consists of a Fickian-like starting period where water diffuses in interstitials/pores without interaction with polarizable groups. This is followed by a case-II-sorption period (linear part) where swelling of the polymer due to interaction with the penetrant takes place (see Fig. 2.18). Prerequisite for the applicability of this model is that the penetrant mobility is much bigger than the polymer segment mobility. This implies that the polymer relaxation controls the uptake under considerable swelling and as a result, the mass uptake proceeds linear with time, forming a sharp front.

If the knowledge of the moisture take-up rate by the coating during early stages of absorption is required, the Brasher-Kingsbury equation [63] is giving a reasonable estimate of the water volume fraction  $\phi(t) = \log[C(t)/C(t=0)]/\log(\epsilon_w)$ , where  $\epsilon_w$  denotes the dielectric constant of water. Nevertheless, non-Fickian (or anomalous) sorption is a common behaviour for coating-water systems below the polymer glass transition temperature  $T_g$  [64]. The slow relaxation of the polymer chains due to the sorption of the water molecules is one reason for the abnormal sorption kinetic: Motions of the entire or parts of the glassy polymer chains are not sufficiently fast to completely homogenize the change of environment as water or other penetrants enter the polymer matrix (see Chap. 5 by Monteux et al. and Chap. 9 by J.-U. Sommer for an introduction into polymer dynamics). Consequently, water molecules or dissolved ions can find their way into “irregular cavities” with different intrinsic diffusional mobility. In such cases, more complex models describing the anomalous diffusion, adapting a suitable effective medium theory for the moisture in the coating, need to be applied [65, 66].

The determination of polarization resistance and interfacial capacitance for coated metals without artificial defects like a scratch is only possible if the impedance of the coating is smaller than or equal to the impedance of the interfacial reaction. For commercial coating systems one can hardly clearly separate the time constants of the interfacial reaction and the polymer film. Thus, the impedance of the interface cannot be deduced from the overall impedance of the polymer-coated metal leaving the analysis of the interface ( $R_P$  and  $C_{DL}$ ) limited to very thin polymers and highly inhibited interfaces or special arrangements by placing the

reference electrode directly at the interface. Another drawback are for instance non-linear effects within the coating systems or electrochemical setups. These are often overcome by using constant phase elements instead of capacitors in equivalent circuits used for fitting of data obtained from industrial coating systems, though there are intrinsic limitations in the interpretation [25, 67, 68].

### 2.4.3 Cathodic Delamination

Coatings with good corrosion protection properties prevent the access of hydrated ions to the coating/metal interface, acting as a barrier. At the interface, such coatings occupy metal or oxide adsorption sites. Thereby, the water activity at the interface is reduced. Although the interfacial ingress of water often weakens the adhesion of the polymer onto the metal therefore reducing the interfacial stability, such wet de-adhesion mechanisms are significantly accelerated and supported by electrochemical corrosion processes like cathodic delamination. Cathodic delamination is one of the—if not even the—fastest failure mechanisms of organically coated metals and a result of an electrochemical cell in which a separation of the anodic and cathodic reaction site takes place. It is the dominant corrosion mechanism in atmospheres with high humidity for coated metals like iron or zinc, which are covered by conductive oxide structures. Depending on the nature of the metallic substrate, the stability of the coating/metal interface against cathodic delamination is mainly determined by several properties [47, 69–71]:

1. The electron-transfer reaction at the interface between polymer and metal.
2. The redox reaction of the metallic oxide between the metal and the coating.
3. The chemical stability of the interface with respect to the reaction products of the electron transfer reaction.
4. The oxygen transport through the organic coating or defects.

Taking these four factors into account, distinct differences between the three most relevant technical surfaces must be expected:

- Steel: Basically iron, with low band-gap oxides which are highly electron conducting and stable in alkaline media.
- Galvanized Steel (Z, ZE): Basically zinc, with semiconducting oxides, which are not stable in alkaline media.
- Aluminium: High band-gap semiconducting oxides, which act as insulator and are not stable in alkaline media.

Cathodic delamination starts with randomly distributed anodes and cathodes in a blister-like defect or at a delaminated area [72]. It is a type of reaction that dominates on polymer/metal interfaces of metals covered by electron conducting or semiconducting oxides with a low band-gap in the presence of coating defects. The determining factors for cathodic delamination are the electrochemical and pH-stability of the metal oxide, the oxygen permeability and adhesion of the

organic coating, the kind of electrolyte in the defect, as well as the relative humidity of the surrounding atmosphere.

As discussed in Sect. 2.2.2, the kinetics of cathodic delamination can be investigated by means of SKP measurements and basically two potential levels characterise the SKP profiles measured during delamination in the presence of oxygen and moisture. At and close to the defect, the measured potential is considerably more negative due to the anodic dissolution of the metal (see Fig. 2.19). When iron is taken as an example, oxygen will be reduced ( $\text{O}_2 + 2\text{H}_2\text{O} + 4\text{e}^- \rightarrow 4\text{OH}^-$ ) in the defect area until the diffusion limiting current density level is reached. Iron dissolves as anodic counter reaction in the defect [69, 70].

Initial oxygen reduction also occurs at the intact coating/metal interface, but it is kinetically strongly inhibited. The intact interface is characterized by a high electronic conductivity of the oxide-covered iron surface, which allows electron transfer but due to the presence of the adhering polymer no ion transfer reactions. Therefore, the oxidation of iron oxide acts as the anodic counter reaction to the oxygen reduction. Consequently, a fast reduction of donor density within the oxide is observed, resulting in a decreasing rate of the electron transfer reaction and an anodic shift of the interfacial potential. As a consequence, above a certain anodic potential, the rate of oxygen reduction is extremely small, and no further anodic potential shift is observed. This is the actual potential as measured by the SKP in the area of an intact coating [43–45].

As discussed above, a distinct potential step between defect area and intact interface is monitored by SKP measurements. For most coatings, this sudden change in potential marks the delamination front and is the most interesting feature because at this location those processes responsible for the loss of adhesion of the coating occur [43–45]. This steep step in the potential originates from the migration of hydrated ions: The electrolyte in the defect can penetrate into the adjacent intact polymer/metal interface. Thereby the kinetic barrier for oxygen reduction at the intact interface will be bypassed and a galvanic couple between two formerly isolated electrochemical cells is established. In order to compensate the local charge (due to the oxygen reduction) at the delamination front, soluble cations of the electrolyte in the defect are electrostatically attracted. These ions have to be

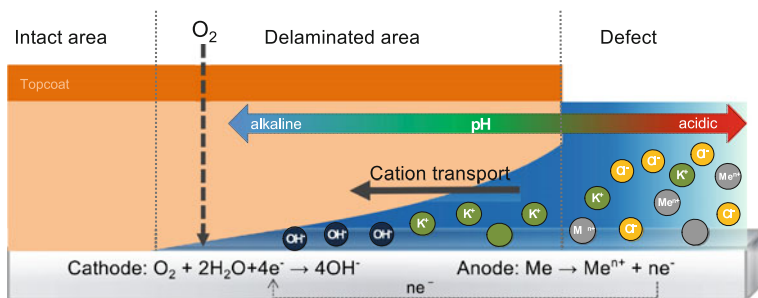


**Fig. 2.19** Schematic illustration of the mechanism of cathodic delamination

transported either by migration or diffusion to the zone of oxygen reduction. Additionally, in the delamination zone, corrosive anions like chlorides are repelled by the negative charge of generated hydroxide ions.

During oxygen reduction, a strongly alkaline electrolyte is formed, with several consequences. Because interfacial iron dissolution is still inhibited, the iron surface becomes passivated. Further, the oxidative degradation of the polymer at the interface, either by the generated hydroxide ions, or by highly reactive oxygen species (in particular radicals or other intermediates evolved in the oxygen reduction reaction, see e.g. [73, 74]), results in delamination of the organic coating only by bond breaking within the organic coating near the interface. It is still an open question which bond actually breaks [51].

The nature of cathodic delamination, especially the separation of local anode (iron dissolution within the defect) and local cathode (oxygen reduction within the delaminated area) requires a transfer of electrons as well as hydrated cations to the electrolyte front position. For many coating systems, the interfacial ion transport represents the slowest process step and therefore is rate-determining. In such cases, the delamination scales with the square root of time. However, especially in the presence of novel pre-treatments, highly cross-linked plasma polymers or e-coats, the rate determining step is reaction controlled, either by limiting the electron transfer or the oxygen reduction reaction. As a consequence, the delamination scales are linear with time. Details of analyses of the different regimes are found in the literature [51, 75].

As pointed out above, a strongly alkaline electrolyte is formed during oxygen reduction. Compared to iron or cold rolled steel, the oxides of zinc present on galvanized steel are less stable within such an alkaline environment. Although the basic mechanisms of cathodic delamination are similar to iron, additional anodic reactions in the section of interfacial ion transport are present, especially if the defect consists of iron [75–77]. On the one hand, zinc cathodically protects the underlying steel. On the other hand, this anodic process is attributed to amphoteric properties of zinc oxide. Although zinc also gets passivated in alkaline environments,  $\text{Zn}(\text{OH})_2$  tends to dissolve as zincate as the pH increases [78]. In the defect area, this is hardly of relevance for the delamination process, but within the section of interfacial ion transport, distinct oxide growth is reported for ongoing delamination at polymer/zinc interfaces by dissolution/precipitation of  $\text{Zn}(\text{OH})_2$  [75–77, 79].

The difference between cathodic delamination on iron or mild steel and corrosive delamination at zinc or galvanized surfaces can be visually observed: Within the delaminated area, mild steel remains shiny, whereas galvanized surfaces expose white colored zinc corrosion products. In summary, cathodic delamination requires electron conducting oxides, interfaces, which allow electrochemical reactions like the oxygen reduction reaction, and interfacial transport of hydrated cations. Therefore, cathodic delamination will dominate for substrates such as steel or galvanized steel at high relative humidity. At low humidity and in the presence of insulating oxides like those of magnesium or aluminium alloy grades, cathodic disbonding cannot occur and anodic driven de-adhesion reactions like filiform corrosion will prevail.

## 2.5 Smart Coatings for Active Corrosion Protection

The mechanism of passive corrosion protection, namely the existence of a diffuse double layer and blocking of electrochemical reactions at the interface, have been discussed in Sect. 2.4, together with the mechanism of organic coating failure. Modern coatings systems may contain layers where the onset of corrosion triggers release of corrosion inhibitors. In fundamental research, a number of triggering mechanisms are currently investigated. Examples include a change of pH, ionic strength or the change of electrode potential. Recent developments in the field of intelligent coatings for active corrosion protection will be summarised in this section. Further reading is available in current reviews [80–84].

### 2.5.1 Ionic Strength and pH Triggered Release

Electrochemically driven corrosion processes need—besides electron-transfer reactions—also the counterbalance of ionic charges (see Sect. 2.4.3). Therefore, the corrosion rate is faster if the metal is in contact with an electrolyte with high ion concentration at equivalent pH and temperature. Furthermore, corrosion of metals is always accompanied by local pH changes. While the pH in the vicinity of local anodes is lower due to hydrolysis of solvated metal cations, the pH at local cathodes is predominantly alkaline. Smart coatings releasing inhibitors due to the environmental ion concentration change or change in pH are actually indirectly responding to an onset of corrosion.

Interesting concepts using “ion-sensing” materials as a part of a binder coating system have been introduced. Ion-sensing materials contain naturally existing or synthesised ion-exchange materials and nano-carriers either modified or made of layer-by-layer assembled polyelectrolytes [84–89].

Ion-exchange materials can be divided into cation and anion exchange materials [90, 91]. Cation exchange materials can carry corrosion inhibiting cations, which are known to inhibit the oxygen reduction reaction (e.g.  $\text{Ce}^{3+}$ ,  $\text{Zn}^{2+}$ , rare earth cations). Zeolite and bentonite clays and cross-linked polystyrene-sulphonate are the materials of choice for storing cationic inhibitors. Excellent corrosion inhibition and especially cathodic delamination inhibiting properties have been shown, if such materials have been applied as pigments in a coating matrix. The mechanism of release is due to the interaction of cations from a corrosive electrolyte with the pigments, leading to an exchange of the cations from the electrolyte with the corrosion inhibiting cation in the pigments. The corrosion inhibiting cation can form insoluble complexes with hydroxide ions, which can precipitate and block preferentially the cathodic reaction.

The predominantly investigated anion exchange pigment is layered double hydroxide compounds like hydrotalcite (HT). The structure consists of



metal-hydroxide layers with excess positive charges, where anions are stored in between the layers to compensate the positive charges. The mechanism of release is similar as for the cation exchange pigments, but with the only difference that in this case aggressive anions like chloride are removed from the electrolyte and are adsorbed inside the HT, while the inhibitors are released. The use of pigments as part of a corrosion inhibiting primer coating on aluminium alloys has investigated in depth [84, 92, 93].

The advantage of ion-exchange materials is their very fast response and release of inhibitors. However, for a prolonged corrosion protection, fast releasing and slow releasing nano-carriers are needed in a combination in a coating formulation [94].

There is almost no limit in giving organic polymeric materials desired functionality for the application in corrosion protection. Very successfully applied polymer classes are polyelectrolytes, which on the one hand have been used for sensing the change in ionic-strength and on the other hand to sense also pH changes during corrosion. Three important strategies have been followed [88, 95, 96]:

1. The storage of inhibitors inside polyelectrolyte coatings.
2. Encapsulation and surface modification of hollow nano materials bearing corrosion inhibitors with polyelectrolytes.
3. Preparation of hollow polyelectrolyte capsules, with corrosion inhibitors encapsulated inside the core.

The layer-by-layer polyelectrolyte assembly provides an inexpensive and robust method to build coatings that are water resistant and stable, even at high ionic strength and in acidic and basic media over a wide range of temperature, pH and solvent changes. Polyelectrolyte multilayers built by layer-by-layer assembly can be deposited on several metal substrates such as gold, stainless steel, iron, aluminium, titanium, nickel, silver, copper, and zinc.

Examples of a negatively-charged polyelectrolytes include polyelectrolytes comprising a sulfonate group ( $-\text{SO}_3^-$ ). Examples include poly(styrene sulfonic acid), poly(2-acrylamido-2-methyl-1-propane sulfonic acid), sulfonated poly(ether ether ketone), polycarboxylates such as poly(acrylic acid), and poly(methacrylic acid). Examples of positively-charged polyelectrolytes include polyelectrolytes comprising a quaternary ammonium group such as poly(diallyldimethylammonium chloride), poly(vinylbenzyltrimethylammonium halogenides), 2-dimethylaminoethyl metacrylate or polyelectrolytes containing a pyridinium group, such as poly(N-methylvinylpyridine).

By changing the type and number of layer-by-layer deposited polyelectrolytes, the responsiveness to corrosion stimuli can be adjusted and engineered. In [97] the surface of inhibitor filled mesoporous silica particles are modified with different combination of polyelectrolytes. While for example the combination of strong polyelectrolytes results in a polymer shell which releases the inhibitors due to the change in ionic strength, the combination of weak polyelectrolytes results in a polymer shell which is pH responsive and releases the inhibitors at alkaline or acidic pH.

Polyelectrolyte complexes have also been used in the development of self-healing matrix coatings. In this case corrosion inhibitors are incorporated as a second component in the complex. The general concept of these films is to entrap the inhibitor into the depot, between one layer and another, from which it can be released only when the corrosion starts. The inhibitor-loaded depot system is then impregnated into the standard corrosion protecting film. Corrosion is accompanied by local changes of the pH, flux of the corrosion products, corrosive species, and of the electrochemical potential. Hence, if the release properties of the inhibitor depot can be affected by any of the reactions accompanying the corrosion process, the release of the entrapped inhibitor is initiated by the corrosion process itself. Polyelectrolyte coatings and complexes are sensitive to pH changes in a local area and can influence very effectively the depot of the corrosion inhibitors and their release due to pH fluctuations during the corrosion process [88].

### 2.5.2 *Electrode Potential Triggered Release*

While the change in pH and ionic strength are an indirect indication that corrosion takes place, the change of the electrode potential of a metal is a direct, reliable and the most case-selective indicator for a corrosion process. The electrode potential of every non-inert metal is always and only decreasing when corrosion occurs.

Conducting polymers (CP) are an excellent material of choice for sensing the corrosion potential change and for storing and releasing inhibitors.

CP consist of conjugated chains containing  $\pi$ -electrons delocalised along the polymer backbone. In their natural form, conductive polymers are semiconducting materials that can be doped and converted into electrically conductive forms. The doping can be either oxidative or reductive, though oxidative doping is more common. Herein, some part of the polymer backbone is getting positively charged and counterbalanced by anions (which can be also corrosion inhibitors). There are generally two states of CP: non-conducting (uncharged/reduced state) and oxidized (p-doped/oxidized and the most stable state) where electrons are removed from the backbone [98]. The doping processes are usually reversible and typical conductivities can be switched between those of insulators (less than  $10^{-10}$  S cm<sup>-1</sup>) and those of metals ( $10^5$  S cm<sup>-1</sup>). Almost all of the conductive polymers used in corrosion protection fall into one of the following classes: polyanilines, polyheterocycles and poly(phenylene vinylenes).

The most widely studied of the intrinsically conducting polymers (ICPs) for corrosion protection coatings has been polyaniline (PANI). The advantages of this material are (i) easy chemical and electrochemical polymerisation, (ii) easy doping and de-doping by treatment with aqueous acids and bases and (iii) its high resistance to environmental degradation [99]. PANI is usually prepared in the emeraldine salt form by oxidative polymerisation of aniline in acidic environment. While there is general agreement that PANI performs well in preventing corrosion, the mechanism of this process is still under investigation. Several hypotheses have been

suggested for the mechanism of corrosion protection using conductive polymers, specifically PANI: (i) PANI contributes to the formation of an electrical field at the metal surface, restricting the flow of electrons from metal to oxidant; (ii) PANI forms a dense, strongly adherent, low-porosity film similar to a barrier coating; and (iii) PANI causes the formation of protective layers of metal oxides on a metal surface. However, PANI possesses the important disadvantage that it is insoluble in the majority of solvents, making its processing very difficult [100].

One of the features which makes use of CP attractive for pigment coatings is the fact that corrosion inhibitor anions can be stored as counter ions in the oxidized polymer backbone. These anions can be released upon the onset of corrosion and the subsequent reduction of CP. Considerable research has been conducted on CP for corrosion protection, however there are four crucial points which have to be generally taken into consideration for designing potential triggered release systems based on CP [101–106]:

1. The efficiency of release of anionic inhibitors is based on their ionic mobility and has to compete with cation incorporation in the CP, which is usually the preferred situation.
2. Due to fast cation incorporation, electropolymerized CP films with continuous ionic networks may even enhance corrosion and can lead to a fast breakdown of the coating system. This means the direct electrochemical synthesis of PANI on a metal surface has to be ruled out for corrosion protection applications.
3. Only negatively charged molecules with non-oxidizable groups and with high solubility in acidic environment can be used as dopants for CP. However, corrosion inhibitors like mercaptobenzothiazole are not soluble in acidic environment and the thiol functional group can be easily oxidized in the oxidative environment used to synthesise conducting polymers.
4. CPs applied especially on zinc tend to react with the metal. Consequently, metal and CP are usually electronically decoupled (Fermi-level misalignment) and the CP loses its capability to sense the potential changes of the metal, due to the formation of an insulating layer between CP and zinc.

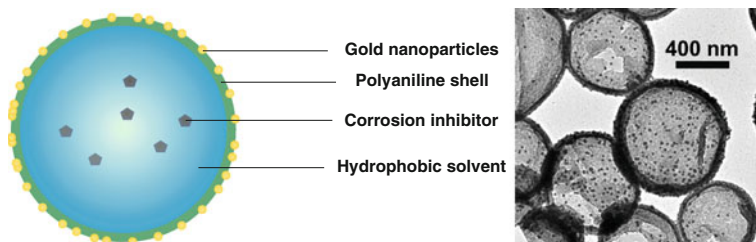
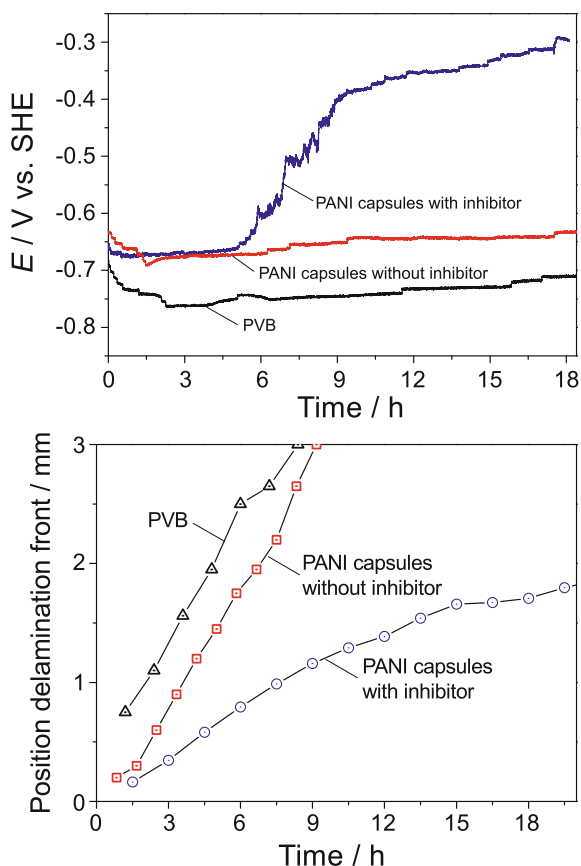


**Fig. 2.20** Schematic depiction of the release concept based on PANI capsules and the corresponding TEM micrograph of a PANI capsule synthesised via miniemulsion technique and decorated with gold nanoparticles

In a recent work [107] these challenges in using conducting polymers have been addressed, and a novel structure for storing and releasing inhibitors has been introduced (Fig. 2.20). The new structure synthesised by the miniemulsion technique comprises a redox-sensitive PANI shell and a corrosion inhibitor (3-nisa/3-nitrosalicylic acid) encapsulated in the hydrophobic (ethylenebenzene/hexadecane) core. Furthermore, the shell is decorated by gold nanoparticles to circumvent electronic decoupling of the capsules from the metal surface (Fig. 2.20).

If the capsules are formulated with a non conducting coating and applied as a composite coating on zinc, they show a self-healing behaviour of a defect. The corrosion potential has been recorded by SKP and indicates that a scratch can be passivated by a coating containing the PANI capsules with inhibitors. On the other hand, the capsules without inhibitors and the binder coating do not show any kind of passivating effect, Fig. 2.21. Delamination performance measured by SKP unravels that after passivation of the defect the progress of cathodic delamination is completely inhibited for the coating containing the PANI capsules with inhibitor.

**Fig. 2.21** *Top* Corrosion potential monitored by the SKP in an artificial defect down to zinc covered with 1 M KCl. *Bottom* Delamination progress over time for non-selfhealing coatings and the coating containing PANI capsules filled with inhibitor



## 2.6 Conclusion

Overall, relatively simple electrochemical processes lead to degradation of metals, also known as corrosion. To combat corrosion on a technological level, several rather sophisticated methods have been developed. Many of these systems involve at least in one step a soft matter system at an aqueous interface. Especially the modern, active systems of corrosion protection are still areas of active research, and a thorough understanding of polymers at aqueous interfaces is needed for the next generation of corrosion protection systems to become reality.

**Acknowledgments** A.A. and A.E. acknowledge support from the DFG (Deutsche Forschungsgemeinschaft) by grant number ER 601/3-1 within the Priority Program 1640 “Joining by plastic deformation”. J.S.M.O. thanks the Mexican Consejo Nacional de Ciencia y Tecnología (Conacyt) for a scholarship. The authors thank Prof. M. Stratmann for continuous support and Michael Rohwerder for helpful discussions.

## References

1. C.M.A. Brett, A.M.O. Brett. *Electrochemistry—Principles, Methods, and Applications* (Oxford University Press, Oxford, 1993)
2. A.J. Bard, L.R. Faulkner, *Electrochemical Methods: Fundamentals and Applications* (Wiley, New York, 2001)
3. C.H. Hamann, A. Hamnett, W. Vielstich. *Electrochemistry* (Wiley, Weinheim, 1998)
4. Helmut Kaesche, *Corrosion of Metals: Physicochemical Principles and Current Problems* (Springer, Berlin, 2003)
5. R.W. Revie (ed.), *Uhlig’s Corrosion Handbook*, 3rd edn. (Wiley, Hoboken, 2011)
6. D.F. Evans, H. Wennerström. *The Colloidal Domain* (Wiley, New York, 1999)
7. Tosaka. [https://en.wikipedia.org/wiki/File:Electric\\_double-layer\\_%28BMD\\_model%29\\_NT.PNG](https://en.wikipedia.org/wiki/File:Electric_double-layer_%28BMD_model%29_NT.PNG), August 2008
8. J. Lyklema, *Fundamentals of Interface and Colloid Science*, vol. 2—Solid-Liquid Interfaces (Academic Press, San Diego, 1995)
9. A. Erbe, K. Tauer, R. Sigel, Ion distribution around electrostatically stabilized polystyrene latex particles studied by ellipsometric light scattering. *Langmuir* **23**, 452–459 (2007)
10. R. Okamoto, A. Onuki, Charged colloids in an aqueous mixture with a salt. *Phys. Rev. E* **84**, 051401 (2011)
11. W. Dreyer, C. Gohlke, M. Landstorfer, A mixture theory of electrolytes containing solvation effects. *Electrochem. Commun.* **43**, 75–78 (2014)
12. J. Lyklema, Quest for ionion correlations in electric double layers and overcharging phenomena. *Adv. Colloid Interface Sci.* **147–148**, 205–213 (2009)
13. R.R. Netz, H. Orland, Beyond Poisson-Boltzmann: Fluctuation effects and correlation functions. *Eur. Phys. J. E* **1**, 203–214 (2000)
14. R.R. Netz, Static van der Waals interactions in electrolytes. *Eur. Phys. J. E* **5**, 189–205 (2001)
15. S. Trasatti, The “absolute” electrode potential—the end of the story. *Electrochim. Acta* **35**, 269–271 (1990)
16. W.M. Haynes (ed.), *Handbook of Chemistry and Physics* (CRC Press, Boca Raton, 2014)
17. Carl Wagner, Wilhelm Traud, Über die Deutung von Korrosionsvorgängen durch Überlagerung von elektrochemischen Teilvorgängen und über die Potentialbildung an Mischelektroden. *Z. Elektrochem. Angew. Phys. Chem.* **44**, 391–402 (1938)

18. C.H. Bamford, R.G. Compton (eds.), *Electrode Kinetics: Principles and Methodology* (Elsevier, Amsterdam, 1986)
19. T.J. Kemp, *Southampton Electrochemistry Group—Instrumental Methods in Electrochemistry* (Ellis Horwood, Chichester, 1985)
20. M. Stern, A.L. Geary, Electrochemical polarization: I. A theoretical analysis of the shape of polarization curves. *J. Electrochem. Soc.* **104**, 56–63 (1957)
21. R.A. Marcus, Electron transfer reactions in chemistry. Theory and experiment. *Rev. Mod. Phys.* **65**, 599–610 (1993)
22. D.D. Macdonald, Reflections on the history of electrochemical impedance spectroscopy. *Electrochim. Acta* **51**, 1376–1388 (2006)
23. A. Battistel, F. La Mantia, Nonlinear analysis: the intermodulated differential immittance spectroscopy. *Anal. Chem.* **85**, 6799–6805 (2013)
24. J.W. Schultze, A.W. Hassel, in *Encyclopedia of Electrochemistry*. Passivity of Metals, Alloys and Semiconductors, vol 4 (Wiley, Weinheim, 2007), pp. 216–235
25. S.-L. Wu, M.E. Orazem, B. Tribollet, V. Vivier, The influence of coupled faradaic and charging currents on impedance spectroscopy. *Electrochim. Acta* **131**, 3–12 (2014)
26. M.E. Orazem, B. Tribollet, *Electrochemical Impedance Spectroscopy* (Wiley, Hoboken, 2008)
27. E. Barsoukov, JR Macdonald, *Impedance Spectroscopy—Theory, Experiment and Applications* (Wiley, Hoboken, 2005)
28. M. Stratmann, The investigation of the corrosion properties of metals, covered with adsorbed electrolyte layers—a new experimental technique. *Corros. Sci.* **27**, 869–872 (1987)
29. S. Yee, R.A. Oriani, M. Stratmann, Application of a Kelvin microprobe to the corrosion of metals in humid atmospheres. *J. Electrochem. Soc.* **138**, 55–61 (1991)
30. K. Wapner, B. Schoenberger, M. Stratmann, G. Grundmeier, Height-regulating scanning kelvin probe for simultaneous measurement of surface topology and electrode potentials at buried polymer/metal interfaces. *J. Electrochem. Soc.* **152**, E114–E122 (2005)
31. M. Stratmann, H. Streckel, On the atmospheric corrosion of metals which are covered with thin electrolyte layers—I. Verification of the experimental technique. *Corros. Sci.* **30**, 681–696 (1990)
32. M. Stratmann, H. Streckel, On the atmospheric corrosion of metals which are covered with thin electrolyte layers—II. Experimental results. *Corros. Sci.* **30**, 697–714 (1990)
33. M. Stratmann, H. Streckel, K.T. Kim, S. Crockett, On the atmospheric corrosion of metals which are covered with thin electrolyte layers-III. The measurement of polarisation curves on metal surfaces which are covered by thin electrolyte layers. *Corros. Sci.* **30**, 715–734 (1990)
34. M. Stratmann, R. Feser, A. Leng, Corrosion protection by organic films. *Electrochim. Acta* **39**, 1207–1214 (1994)
35. M. Stratmann, A. Leng, W. Fürbeth, H. Streckel, H. Gehmecker, K.-H. Große-Brinkhaus, The scanning Kelvin probe; a new technique for the in situ analysis of the delamination of organic coatings. *Prog. Org. Coat.* **27**, 261–267 (1996)
36. H. Baumgärtner, H.D. Liess, Micro Kelvin probe for local work-function measurements. *Rev. Sci. Instr.* **59**, 802–805 (1988)
37. M.F. Becker, A.F. Stewart, J.A. Kardach, A.H. Guenther, Surface charging in laser damage to dielectric surfaces and thin films. *Appl. Opt.* **26**, 805–812 (1987)
38. D. Mao, A. Kahn, M. Marsi, G. Margaritondo, Synchrotron-radiation-induced surface photovoltage on GaAs studied by contact-potential-difference measurements. *Phys. Rev. B* **42**, 3228–3230 (1990)
39. P. Chiaradia, J.E. Bonnet, M. Fanfoni, C. Goletti, G. Lampel, Schottky barrier and surface photovoltage induced by synchrotron radiation in GaP(110)/Ag. *Phys. Rev. B* **47**, 13520–13526 (1993)
40. H. Ren, H. Sinha, A. Sehgal, M.T. Nichols, G.A. Antonelli, Y. Nishi, J.L. Shohet, Surface potential due to charge accumulation during vacuum ultraviolet exposure for high-k and low-k dielectrics. *Appl. Phys. Lett.* **97**, 072901 (2010)

41. J.L. Lauer, J.L. Shohet, Surface potential measurements of vacuum ultraviolet irradiated  $\text{Al}_2\text{O}_3$ ,  $\text{Si}_3\text{N}_4$ , and  $\text{SiO}_2$ . *IEEE Trans. Plasma Sci.* **33**, 248–249 (2005)
42. B. Salgin, D. Pontoni, D. Vogel, H. Schroder, P. Keil, M. Stratmann, H. Reichert, M. Rohwerder, Chemistry-dependent x-ray-induced surface charging. *Phys. Chem. Chem. Phys.* **16**, 22255–22261 (2014)
43. A. Leng, H. Streckel, M. Stratmann, The delamination of polymeric coatings from steel. Part 1: calibration of the Kelvin probe and basic delamination mechanism. *Corros. Sci.* **41**, 547–578 (1998)
44. A. Leng, H. Streckel, M. Stratmann, The delamination of polymeric coatings from steel. Part 2: first stage of delamination, effect of type and concentration of cations on delamination, chemical analysis of the interface. *Corros. Sci.* **41**, 579–597 (1998)
45. A. Leng, H. Streckel, K. Hofmann, M. Stratmann, The delamination of polymeric coatings from steel. Part 3: effect of the oxygen partial pressure on the delamination reaction and current distribution at the metal/polymer interface. *Corros. Sci.* **41**, 599–620 (1998)
46. G.S. Frankel, M. Stratmann, M. Rohwerder, A. Michalik, B. Maier, J. Dora, M. Wicinski, Potential control under thin aqueous layers using a Kelvin probe. *Corros. Sci.* **49**, 2021–2036 (2007)
47. G. Grundmeier, W. Schmidt, M. Stratmann, Corrosion protection by organic coatings: electrochemical mechanism and novel methods of investigation. *Electrochim. Acta* **45**, 2515–2533 (2000)
48. G. Williams, H.N. McMurray, Polyaniline inhibition of filiform corrosion on organic coated AA2024-T3. *Electrochim. Acta* **54**, 4245–4252 (2009)
49. R. Posner, P.R. Sundel, T. Bergman, P. Roose, M. Heylen, G. Grundmeier, P. Keil, UV-curable polyester acrylate coatings: barrier properties and ion transport kinetics along polymer/metal interfaces. *J. Electrochem. Soc.* **158**, C185–C193 (2011)
50. G. Frankel, M. Rohwerder, in *Encyclopedia of Electrochemistry*. Electrochemical Techniques for Corrosion, vol 4 (Wiley, Weinheim, Germany, 2007), pp. 687–723
51. D. Iqbal, J. Rechmann, A. Sarfraz, A. Altin, G. Genchev, A. Erbe, Synthesis of ultrathin poly (methyl methacrylate) model coatings bound via organosilanes to zinc and investigation of their delamination kinetics. *ACS Appl. Mater. Interfaces* **6**, 18112–18121 (2014)
52. N.W. Khun, G.S. Frankel, Effects of surface roughness, texture and polymer degradation on cathodic delamination of epoxy coated steel samples. *Corros. Sci.* **67**, 152–160 (2013)
53. D. Iqbal, R.S. Moirangthem, A. Bashir, A. Erbe, Study of polymer coating delamination kinetics on zinc modified with zinc oxide of different morphologies. *Mater. Corros.* **65**, 370–375 (2014)
54. A. Goldschmidt, H. Streitberger, *BASF-Handbuch Lackiertechnik* (Vincentz, Hannover, 2002)
55. B. Tieke, *Makromolekulare Chemie* (Wiley, Weinheim, 1997)
56. D. Braun, H. Cherdron, H. Ritter, *Praktikum der Makromolekularen Stoffe* (Wiley, Weinheim, 1999)
57. G. Grundmeier, A. Simões, in *Encyclopedia of Electrochemistry*. Corrosion Protection by Organic Coatings, vol 4 (Wiley, Weinheim, Germany, 2007), pp. 500–566
58. F. Deflorian, S. Rossi, M. Fedel, Organic coatings degradation: comparison between natural and artificial weathering. *Corros. Sci.* **50**, 2360–2366 (2008)
59. E.P.M. van Westing, G.M. Ferrari, J.H.W. de Wit, The determination of coating performance with impedance measurements—III. In situ determination of loss of adhesion. *Corros. Sci.* **36**, 979–994 (1994)
60. E.P.M. van Westing, G.M. Ferrari, J.H.W. de Wit, The determination of coating performance with impedance measurements—I. Coating polymer properties. *Corros. Sci.* **34**, 1511–1530 (1993)
61. J.R. Scully, S.T. Hensley, Lifetime prediction for organic coatings on steel and a magnesium alloy using electrochemical impedance methods. *Corrosion* **50**, 705–716 (1994)
62. F. Mansfeld, Use of electrochemical impedance spectroscopy for the study of corrosion protection by polymer coatings. *J. Appl. Electrochem.* **25**, 187–202 (1995)

63. D.M. Brasher, A.H. Kingsbury, Electrical measurements in the study of immersed paint coatings on metal. I. Comparison between capacitance and gravimetric methods of estimating water-uptake. *J. Appl. Chem.* **4**, 62–72 (1954)
64. R. Posner, K. Wapner, S. Amthor, K.J. Roschmann, G. Grundmeier, Electrochemical investigation of the coating/substrate interface stability for styrene/acrylate copolymer films applied on iron. *Corros. Sci.* **52**, 37–44 (2010)
65. B.R. Hinderliter, S.G. Croll, Simulation of transient electrochemical impedance spectroscopy due to water uptake or oxide growth. *Electrochim. Acta* **54**, 5344–5352 (2009)
66. V. La Saponara, Environmental and chemical degradation of carbon/epoxy and structural adhesive for aerospace applications: Fickian and anomalous diffusion, Arrhenius kinetics. *Compos. Struct.* **93**, 2180–2195 (2011)
67. B. Hirschorn, M.E. Orazem, B. Tribollet, V. Vivier, I. Frateur, M. Musiani, Determination of effective capacitance and film thickness from constant-phase-element parameters. *Electrochim. Acta* **55**, 6218–6227 (2010)
68. M.R.S. Abouzari, F. Berkemeier, G. Schmitz, D. Wilmer, On the physical interpretation of constant phase elements. *Solid State Ionics* **180**, 922–927 (2009)
69. U. Stimming, J.W. Schultze, The capacity of passivated iron electrodes and the band structure of the passive layer. *Ber. Bunsenges.* **80**, 1297–1302 (1976)
70. U. Stimming, J.W. Schultze, A semiconductor model of the passive layer on iron electrodes and its application to electrochemical reactions. *Electrochim. Acta* **24**, 859–869 (1979)
71. S. Yee, R.A. Oriani, M. Stratmann, Application of a Kelvin microprobe to the corrosion of metals in humid atmospheres. *J. Electrochem. Soc.* **138**, 55–61 (1991)
72. H. Leidheiser Jr., W. Wang, L. Igetoft, The mechanism for the cathodic delamination of organic coatings from a metal surface. *Prog. Org. Coat.* **11**, 19–40 (1983)
73. S. Nayak, P.U. Biedermann, M. Stratmann, A. Erbe, A mechanistic study of the electrochemical oxygen reduction on the model semiconductor n-Ge(100) by ATR-IR and DFT. *Phys. Chem. Chem. Phys.* **15**, 5771–5781 (2013)
74. S. Nayak, P.U. Biedermann, M. Stratmann, A. Erbe, In situ infrared spectroscopic investigation of intermediates in the electrochemical oxygen reduction on n-Ge (100) in alkaline perchlorate and chloride electrolyte. *Electrochim. Acta* **106**, 472–482 (2013)
75. W. Fürbeth, M. Stratmann, The delamination of polymeric coatings from electrogalvanised steel—a mechanistic approach. Part 1: delamination from a defect with intact zinc layer. *Corros. Sci.* **43**, 207–227 (2001)
76. W. Fürbeth, M. Stratmann, The delamination of polymeric coatings from electrogalvanized steel—a mechanistic approach. Part 2: delamination from a defect down to steel. *Corros. Sci.* **43**, 229–241 (2001)
77. W. Fürbeth, M. Stratmann, The delamination of polymeric coatings from electrogalvanized steel—a mechanistic approach.: Part 3: delamination kinetics and influence of CO<sub>2</sub>. *Corros. Sci.* **43**, 243–254 (2001)
78. M. Pourbaix, *Atlas of Electrochemical Equilibria in Aqueous Solutions*. (National Association of Corrosion Engineers/Centre Belge d'Etude de la Corrosion CEBELCOR, Houston/Bruxelles, 1974)
79. D. Iqbal, A. Kostka, A. Bashir, A. Sarfraz, Y. Chen, A.D. Wieck, A. Erbe, Sequential growth of zinc oxide nanorod arrays at room temperature via a corrosion process: application in visible light photocatalysis. *ACS Appl. Mater. Interfaces* **6**, 18728–18734 (2014)
80. S.J. Garcia, H.R. Fischer, S. van der Zwaag, A critical appraisal of the potential of self healing polymeric coatings. *Prog. Org. Coat.* **72**, 211–221 (2011)
81. A.E. Hughes, I.S. Cole, T.H. Muster, R.J. Varley, Designing green, self-healing coatings for metal protection. *NPG Asia Mater.* **2**, 143–151 (2010)
82. M.F. Montemor, Functional and smart coatings for corrosion protection: a review of recent advances. *Surf. Coat. Technol.* **258**, 17–37 (2014)
83. M. Zheludkevich, in *Self-Healing Materials—Fundamentals, Design Strategies, and Applications*. Self-Healing Anticorrosion Coatings, Chapter 4 (Wiley, Weinheim, 2009), pp. 101–139



84. M.L. Zheludkevich, J. Tedim, M.G.S. Ferreira, "Smart" coatings for active corrosion protection based on multi-functional micro and nanocontainers. *Electrochim. Acta* **82**, 314–323 (2012)
85. D.V. Andreeva, D. Fix, H. Möhwald, D.G. Shchukin, Self-healing anticorrosion coatings based on pH-sensitive polyelectrolyte/inhibitor sandwichlike nanostructures. *Adv. Mater.* **20**, 2789–2794 (2008)
86. B. Blaiszik, S. Kramer, S. Olugebefola, J. Moore, N. Sottos, S. White, Self-healing polymers and composites. *Ann. Rev. Mater. Res.* **40**, 179–211 (2010)
87. S.J. Garcia, H.R. Fischer, P.A. White, J. Mardel, Y. Gonzalez-Garcia, J.M.C. Mol, A.E. Hughes, Self-healing anticorrosive organic coating based on an encapsulated water reactive silyl ester: synthesis and proof of concept. *Prog. Org. Coat.* **70**, 142–149 (2011)
88. D.O. Grigoriev, K. Köhler, E. Skorb, D.G. Shchukin, H. Möhwald, Polyelectrolyte complexes as a smart depot for self-healing anticorrosion coatings. *Soft Matter* **5**, 1426–1432 (2009)
89. M.L. Zheludkevich, D.G. Shchukin, K.A. Yasakau, H. Möhwald, M.G.S. Ferreira, Anticorrosion coatings with self-healing effect based on nanocontainers impregnated with corrosion inhibitor. *Chem. Mater.* **19**, 402–411 (2007)
90. G. Williams, S. Geary, H.N. McMurray, Smart release corrosion inhibitor pigments based on organic ion-exchange resins. *Corros. Sci.* **57**, 139–147 (2012)
91. G. Williams, H.N. McMurray, Inhibition of filiform corrosion on organic-coated AA2024-T3 by smart-release cation and anion-exchange pigments. *Electrochim. Acta* **69**, 287–294 (2012)
92. R.G. Buchheit, H. Guan, S. Mahajanam, F. Wong, Active corrosion protection and corrosion sensing in chromate-free organic coatings. *Prog. Org. Coat.* **47**, 174–182 (2003)
93. G. Williams, H.N. McMurray, M.J. Loveridge, Inhibition of corrosion-driven organic coating disbondment on galvanised steel by smart release group II and Zn(II)-exchanged bentonite pigments. *Electrochim. Acta* **55**, 1740–1748 (2010)
94. M.F. Montemor, D.V. Snihirova, M.G. Taryba, S.V. Lamaka, I.A. Kartsonakis, A.C. Balaskas, G.C. Kordas, J. Tedim, A. Kuznetsova, M.L. Zheludkevich, M.G.S. Ferreira, Evaluation of self-healing ability in protective coatings modified with combinations of layered double hydroxides and cerium molybdate nanocontainers filled with corrosion inhibitors. *Electrochim. Acta* **60**, 31–40 (2012)
95. D.G. Shchukin, M. Zheludkevich, K. Yasakau, S. Lamaka, M.G.S. Ferreira, H. Möhwald, Layer-by-layer assembled nanocontainers for self-healing corrosion protection. *Adv. Mater.* **18**, 1672–1678 (2006)
96. D.G. Shchukin, S.V. Lamaka, K.A. Yasakau, M.L. Zheludkevich, M.G.S. Ferreira, H. Möhwald, Active anticorrosion coatings with halloysite nanocontainers. *J. Phys. Chem. C* **112**, 958–964 (2008)
97. D.G. Shchukin, H. Möhwald, Surface-engineered nanocontainers for entrapment of corrosion inhibitors. *Adv. Funct. Mater.* **17**, 1451–1458 (2007)
98. P. Zarras, N. Anderson, C. Webber, D.J. Irvin, J.A. Irvin, A. Guenther, J.D. Stenger-Smith, Progress in using conductive polymers as corrosion-inhibiting coatings. *Radiat. Phys. Chem.* **68**, 387–394 (2003)
99. J.O. Iroh, R. Rajagopalan, Electrochemical polymerization of aniline on carbon fibers in aqueous toluene sulfonate solution. *J. Appl. Polym. Sci.* **76**, 1503–1509 (2000)
100. A.A. Syed, M.K. Dinesan, Review: polyaniline-a novel polymeric material. *Talanta* **38**, 815–837 (1991)
101. G. Paliwoda-Porebska, M. Rohwerder, M. Stratmann, U. Rammelt, L. Duc, W. Plieth, Release mechanism of electrodeposited polypyrrole doped with corrosion inhibitor anions. *J. Solid State Electrochem.* **10**, 730–736 (2006)
102. M. Rohwerder, A. Michalik, Conducting polymers for corrosion protection: What makes the difference between failure and success? *Electrochim. Acta* **53**, 1300–1313 (2007)
103. M. Rohwerder, L.M. Duc, A. Michalik, In situ investigation of corrosion localised at the buried interface between metal and conducting polymer based composite coatings. *Electrochim. Acta* **54**, 6075–6081 (2009)

104. M. Rohwerder, Conducting polymers for corrosion protection: a review. *Int. J. Mater. Res.* **100**, 1331–1342 (2009)
105. M. Rohwerder, S. Isik-Uppenkamp, C.A. Amarnath, Application of the Kelvin Probe method for screening the interfacial reactivity of conducting polymer based coatings for corrosion protection. *Electrochim. Acta* **56**, 1889–1893 (2011)
106. G. Williams, R.J. Holness, D.A. Worsley, H.N. McMurray, Inhibition of corrosion-driven organic coating delamination on zinc by polyaniline. *Electrochem. Commun.* **6**, 549–555 (2004)
107. A. Vimalanandan, L.-P. Lv, T.H. Tran, K. Landfester, D. Crespy, M. Rohwerder, Redox-responsive self-healing for corrosion protection. *Adv. Mater.* **25**, 6980–6984 (2013)

Soft Matter at Aqueous Interfaces

Lang, P.R.; Liu, Y. (Eds.)

2016, VIII, 555 p. 230 illus., 116 illus. in color., Softcover

ISBN: 978-3-319-24500-3